AFRL-RY-WP-TR-2010-1043

INITIAL HIGH-POWER-CW-LASER TESTING OF LIQUID-CRYSTAL OPTICAL PHASED ARRAYS

Edward A. Watson

EO Sensor Technology Division

Bert Whitaker

OptiMetrics, Inc.

Scott Harris

Flatiron Research, LLC

FEBRUARY 2005
Interim Report

AIR FORCE RESEARCH LABORATORY
SENSORS DIRECTORATE
WRIGHT-PATTERSON AIR FORCE BASE, OH 45433-7320
AIR FORCE MATERIEL COMMAND
UNITED STATES AIR FORCE

NOTICE AND SIGNATURE PAGE

Using Government drawings, specifications, or other data included in this document for any purpose other than Government procurement does not in any way obligate the U.S. Government. The fact that the Government formulated or supplied the drawings, specifications, or other data does not license the holder or any other person or corporation; or convey any rights or permission to manufacture, use, or sell any patented invention that may relate to them.

This report was cleared for public release by the USAF 88th Air Base Wing (88 ABW) Public Affairs Office (PAO) and is available to the general public, including foreign nationals. Copies may be obtained from the Defense Technical Information Center (DTIC) (http://www.dtic.mil).

AFRL-RY-WP-TR-2010-1043 HAS BEEN REVIEWED AND IS APPROVED FOR PUBLICATION IN ACCORDANCE WITH ASSIGNED DISTRIBUTION STATEMENT.

*//Signature//

TIMOTHY M. FINEGAN, Project Engineer
EO Combat ID Technology Branch
EO Sensor Technology Division

//Signature//

ROBERT J. FELDMANN, Chief
EO Combat ID Technology Branch
EO Sensor Technology Division

//Signature//

BRIAN C. FORD, Colonel, USAF
Chief, EO Sensor Technology Division
Sensors Directorate

This report is published in the interest of scientific and technical information exchange, and its publication does not constitute the Government's approval or disapproval of its ideas or findings.

*Disseminated copies will show "//Signature//" stamped or typed above the signature blocks.

REPORT DOCUMENTATION PAGE

Form Approved
OMB No. 0704-0188

1. REPORT DATE *(DD-MM-YY)*	2. REPORT TYPE	3. DATES COVERED *(From - To)*
February 2005	Interim	11 December 2003 – 11 December 2004

4. TITLE AND SUBTITLE
INITIAL HIGH-POWER-CW-LASER TESTING OF LIQUID-CRYSTAL OPTICAL PHASED ARRAYS

5a. CONTRACT NUMBER
In-house

5b. GRANT NUMBER

5c. PROGRAM ELEMENT NUMBER
62204F

6. AUTHOR(S)
Edward A. Watson (AFRL/RYJ)
Bert Whitaker (OptiMetrics, Inc.)
Scott Harris (Flatiron Research, LLC)

5d. PROJECT NUMBER
2003

5e. TASK NUMBER
11

5f. WORK UNIT NUMBER
2003112W

7. PERFORMING ORGANIZATION NAME(S) AND ADDRESS(ES)
EO Sensor Technology Division (AFRL/RYJ)
Air Force Research Laboratory Sensors Directorate
Wright-Patterson Air Force Base, OH 45433-7320
Air Force Materiel Command, United States Air Force

OptiMetrics, Inc.

Flatiron Research, LLC

8. PERFORMING ORGANIZATION REPORT NUMBER
AFRL-RY-WP-TR-2010-1043

9. SPONSORING/MONITORING AGENCY NAME(S) AND ADDRESS(ES)
Air Force Research Laboratory
Sensors Directorate
Wright-Patterson Air Force Base, OH 45433-7320
Air Force Materiel Command
United States Air Force

10. SPONSORING/MONITORING AGENCY ACRONYM(S)
AFRL/RYJM

11. SPONSORING/MONITORING AGENCY REPORT NUMBER(S)
AFRL-RY-WP-TR-2010-1043

12. DISTRIBUTION/AVAILABILITY STATEMENT
Approved for public release; distribution unlimited.

13. SUPPLEMENTARY NOTES
PAO Case Number: 88ABW 10-0755; Clearance Date: 23 Feb 2010. This report contains color.

Research on this report was completed in 2005.

14. ABSTRACT
The performance of liquid-crystal phase retarders and optical phased arrays may be gauged by examining their behavior when they are used as variable wave plates. We used this method to evaluate the performance of these devices as they are heated, and as they are exposed to high-power laser energy at 1.083 μm. The results indicate that at higher temperatures or higher power levels of laser exposure, the available phase-modulation depth is reduced, presumably due to heating in both cases. In some instances, normal phase-shifting behavior returned when the conditions of the tests were removed, while in others, the behavior eventually vanished entirely, never to return on its own. We developed a novel method for reviving (as well as extending the temperature range of) the performance of phase retarders after such impairments, by imposing a momentary, DC drive voltage (the "DC Reset"). Also, as the high-power laser was activated (or deactivated), the LCoS (Liquid Crystal on Silicon) OPA's we examined exhibited thermal time constants in the neighborhood of 20 seconds. Petrographic-microscope images were recorded before and after the tests and, in spite of no apparent materials damage, showed LC migration in most of the devices, supposably due to thermal expansion and contraction. Additional petrographic images were recorded to show the visually apparent local phase-shifting behavior of the devices as the laser-energy level was increased.

15. SUBJECT TERMS
Beam Steering, Optical Phased Array, OPA, Wave Plates, Phase Retarders, Phase Shifters, Liquid Crystal, LCoS, Thermal Damage, Laser Damage, DC Reset, Petrographic

16. SECURITY CLASSIFICATION OF:			17. LIMITATION OF ABSTRACT:	18. NUMBER OF PAGES	19a. NAME OF RESPONSIBLE PERSON (Monitor)
a. REPORT	b. ABSTRACT	c. THIS PAGE			Timothy M. Finegan
Unclassified	Unclassified	Unclassified	SAR	44	19b. TELEPHONE NUMBER *(Include Area Code)* N/A

Standard Form 298 (Rev. 8-98)
Prescribed by ANSI Std. Z39-18

Table of Contents

List of Figures iii

List of Tables iv

Acknowledgements v

1. Introduction 1
    1.1. Motivation 1
    1.2. Beam-steering overview 1

2. Experimental concept 4

3. Results 9
    3.1. Reduction of phase-modulation depth with laser exposure 9
        3.1.1. Test 200312292L1 (phase shifter, laser exposure 9
        3.1.2. Test 20040227L1 (spatial light modulator, laser exposure 11
        3.1.3. Laser-exposure-test summary 14
    3.2 Transient behavior of thermal effects 15
    3.3 Reduction of phase-modulation depth with heating 15
        3.3.1. Test 200312193H2 (phase shifter, heating 15
        3.3.2. Test 200312193H3 (phase shifter, heating; the "DC Reset 17
        3.3.3. Test 200312191L1H2 (spatial light modulator, heating 20
        3.3.4. Heating-test summary 23
    3.4. Images through crossed polarizers 24
        3.4.1. Apparent reduction of phase-modulation depth 24
        3.4.2. Apparent damage (reversible in some cases) 26

4. Thermal Modeling 29

5. Conclusions 32
    5.1. Reduction of Phase-Modulation Depth 32
    5.2. Migration of liquid-crystal material 32
    5.3. Summary of Conclusions 34

List of Figures

Figure 1 -- Simplified cross section of a liquid-crystal optical phased array 2
Figure 2 -- Schematic diagram of the LCOPA, high-power-CW-laser testing setup 6
Figure 3 -- Schematic diagram of the layers in an LC-on-silicon device 7
Figure 4 -- 200312292L1: Laser-exposure test of phase shifter 200312292 (increasing power) ...9
Figure 5 -- Unwrapped phase shift for laser-exposure test of phase shifter (increasing power) ..10
Figure 6 -- 200312292L1: Laser-exposure test of phase shifter 200312292 (decreasing power) 10
Figure 7 -- Unwrapped phase shift for laser-exposure test of phase shifter (decreasing power)..11
Figure 8 -- 20040227L1 -- Laser-exposure test of SLM 20040227 (increasing power) 12
Figure 9 -- Unwrapped phase shift for laser-exposure test of SLM (increasing power) 12
Figure 10 -- 20040227L1: Laser-exposure test of SLM 20040227 (decreasing power) 13
Figure 11 -- Unwrapped phase shift for laser-exposure test of SLM (decreasing power)....13
Figure 12 -- Normalized transmission curves for preliminary laser-exposure test of SLM 14
Figure 13 -- Cooling transient in the LCOPA is turned off 15
Figure 14 -- Heating transient in the LCOPA when high-power illumination is turned on 15
Figure 15 -- 200312193H2: Heating test of phase shifter 200312193 (increasing temperature) ..16
Figure 16 -- Unwrapped phase shift for heating test of phase shifter (increasing temperature)....16
Figure 17 -- 200312193H2: Heating test of phase shifter 200312193 (after cooling)....17
Figure 18 -- 200312193H3: Subsequent heating test of phase shifter (increasing temperature)...18
Figure 19 -- Unwrapped phase shift for H3 heating of phase shifter (increasing temperature) 18
Figure 20 -- 200312193H3: Subsequent heating test of phase shifter (decreasing temperature) ..19
Figure 21 -- Unwrapped phase shift for H3 heating of phase shifter (decreasing temperature)....19
Figure 22 -- 200312191L1H2: Heating test of SLM 200312191 (increasing temperature) 21
Figure 23 -- Heating test of SLM (continued) 21
Figure 24 -- Heating test of SLM (continued, and after cooling) 22
Figure 25 -- Unwrapped phase shift for heating test of SLM (increasing temperature)....22
Figure 26 -- Normalized transmission curves for heating test of phase shifter 23
Figure 27 -- A sequence of images of phase shifter (laser power slowly increased)....25
Figure 28 -- Persistent defect in liquid-crystal layer after switching off high-power-laser....26
Figure 29 -- Petrographic-microscope pictures of LC-layer boundary of phase shifter 27
Figure 30 – Nonfunctional void beyond the right edge of the second picture in figure 29 27
Figure 31 -- Petrographic-microscope pictures of LC-layer boundary of SLM 28
Figure 32 -- Simplified heat profile in an LCOPA device 30

List of Tables

Table 1 -- Thermal conductivity for materials in a typical LCOPA 30
Table 2 -- Required heat absorption for a temperature rise across an LCOPA material layer 31

Acknowledgements

The authors would like to thank Steve Serati, Teresa Ewing, and Jay Stockley for their assistance and for supplying the devices examined in this work.

1. Introduction

1.1. Motivation

Today's battlefields are racetracks of technological challenge. One of the most pivotal challenges is ensuring the accurate delivery of missiles (and other such devices) to their targets. In some cases, pilots or ground crews aim a laser beam, which the missile then follows to the intended target. The most common method for aiming these beams involves the use of gimbaled mirrors. However, these mechanisms are plagued by inertial sluggishness, low reliability, and excessive weight. For some time, research has explored alternative, non- or minimally mechanical methods for aiming these laser beams. One possibility is the incorporation of liquid-crystal, optical phased arrays (LCOPA's), in the hope that they will provide relatively quick and reliable beam steering with a significant reduction in the weight of the required components. Almost all the work with these devices to date has focused on demonstrations with a variety of optical configurations in applications using low optical powers, usually via diode lasers or low-power gas lasers such as helium-neon or argon. Since one eventual goal is to incorporate LCOPA's into a variety of high-power-airborne-laser systems such as military active electro-optical systems and other industrial applications, we have begun to examine the properties of liquid-crystal devices when used with high-power pulsed and CW lasers. One of the primary challenges is that, in contrast to most of their mirrored counterparts, when LCOPA's are used to steer laser beams of particularly high powers, their performance often suffers due to localized internal heating.

Here we present the results of our examination of several liquid-crystal devices. Our intention is to explore the capacity of current optical-phased-array technology to manipulate high-power laser energy, and to investigate the nature and onset of the deleterious thermal effects that degrade that capacity.

1.2. Beam-steering overview

One obvious way of aiming a laser beam is to move the entire laser itself. High-powered lasers are often massive and, even at their most rugged, delicate instruments. The difficulty of having to move such a typically massive and fragile object makes this option a bad idea.

It is inevitably simpler to devise a mechanism entirely separate from the laser. Of these, one of the most elementary has a gimbaled mirror, manipulated by three motors – one for each mutually orthogonal axis of motion. This mirror reflects the laser beam in the intended direction through a window in the aircraft or ground-based targeting unit. The mirrors, motors, mounts and other hardware for these devices are so massive that the system as a whole is fraught with prohibitive inertial ramp-up and overshoot effects: the weight causes lengthy response times and impairs the long-term reliability of the system alignment.

Another method uses refraction via rotating (Risley) prisms to steer the beam. Unfortunately, this method is significantly plagued by the same problems as the gimbaled mirror.

Both of these are examples of what is referred to as mechanical beam steering, as they rely on mechanisms to physically align their components.

An alternative to the use of gimbaled mirrors or rotating prisms is that of liquid-crystal optical phased arrays (LCOPA's), the technology of which has been significantly advanced during the past decade. LCOPA technology is an example of non-mechanical beam steering, as it relies only on electrical signals, rather than mechanisms for physical alignment. The basic arrangement of an LCOPA is shown in figure 1. It is constructed essentially like a parallel-plate capacitor: the plates are made of glass with a coating of transparent conductive oxide on the inside surfaces (such as indium-tin-oxide, or ITO). If the coatings are both continuous planes, the device is referred to as a phase retarder, or phase shifter; if one of the coatings has a pattern of rows and columns (pixels), it is referred to as an optical phased array (OPA), or spatial light modulator (SLM).

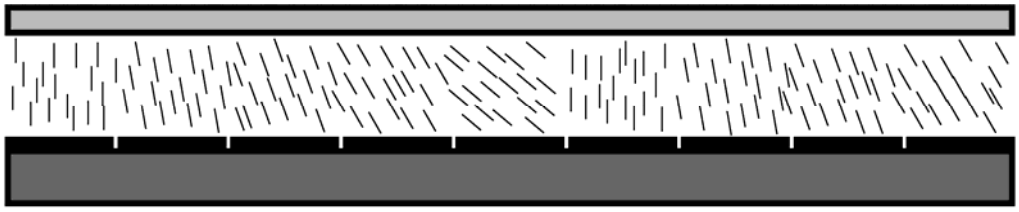

Figure 1: Simplified cross section of a liquid-crystal optical phased array.

In the early stages of assembly, after these conductive films have been applied, a final, polymer alignment layer is deposited on each of the plates over the conductive film. These surfaces are then repeatedly rubbed in a single direction with a cloth. Using small spacer balls or rods, the plates are then assembled with their conductive surfaces facing each other and glued together around most of their perimeter. Via capillary action, a thin layer of liquid-crystal material (after heating it beyond its isotropic temperature) is drawn into the space between the two plates, after which the entire device is sealed and allowed to slowly cool.

In a phase shifter, the entire, two-dimensional section of liquid crystal in the device responds to the voltage applied between the conductive-oxide coatings on the two plates. Simple wire connections are made to both of these full-plate, conductive coatings. In the OPA case, on the other hand, connections for one of the plates are made to each pixel of the patterned coating, so that specific voltages can be applied across each pixel area (to the continuous coating on the other plate) of the liquid crystal in the device.

In a transmissive LCOPA, both substrates are transparent; in a reflective LCOPA, one of the substrates is transparent, the other reflective. In a reflective device, the glass is typically fused silica, and the electrodes typically aluminum, configured as part of a VLSI-silicon backplane that includes other electrical capabilities.

Rubbing the alignment layers on the plates causes the LC molecules nearest those surfaces to align parallel to the direction of the rub, tilting slightly away from the surface when moving along the molecule in that direction. Molecular interactions cause the molecules to align with their neighbors. Coupled with the fact that, in this case, the plates are rubbed in antiparallel directions, this causes a slightly tilted, nematic ordering throughout the cell, with the molecules aligned almost parallel to the plates. As the voltage across a section of the LC is raised, regardless of its polarity, a dipole moment is induced in the molecules there. This generates a torque, tilting them so they are aligned more parallel to the electric field. The higher the voltage (field), the more the molecules are tilted parallel to it.

The reason this tilting is important is that when this LC device is illuminated by a laser beam, the light component whose polarization is oriented with the long (slow) axis of the molecules is slowed down more as the molecules are tilted with their long axes more perpendicular to the propagation direction (at lower voltages). Conversely, this light is slowed down less as the molecules are tilted with their long axes more parallel to the propagation direction (at higher voltages).

In other words, since the liquid-crystal material is birefringent and has a dielectric anisotropy, the local index of refraction for light polarized along one axis may be adjusted by applying different voltages to the array of electrodes behind the liquid-crystal layer.

This means that the pixels of an OPA can be addressed to produce phase-delay patterns that mimic prisms, lenses, and countless other refractive tools. These patterns can be divided into integer-multiple-of-wavelength, phase-ramp resets to allow a greater versatility. In this way, these small devices can be used to steer light beams.

2. Experimental concept

When these devices are illuminated by light whose polarization is neither completely parallel nor completely perpendicular to the long axis of the LC molecules, the resultant polarization of the transmitted (or reflected) light is rotated. This is because the index-of-refraction modulation occurs along only that single axis – the long axis of the LC molecules. The primary metric we use to gauge the performance of these devices is their ability to modulate the phase of the light they reflect – they can be made to behave like variable wave plates. It is this phase-modulating ability that is impaired (or enhanced) when one of the devices is heated or exposed to high-power-laser energy. During each of the tests, the devices were operated as simple phase shifters, and this modulation behavior was recorded.

The samples examined in these tests are reflective, with silvering on the back (and in the case of the SLM's, patterned) plate. Boulder Nonlinear Systems supplied the samples which, as mentioned before, have their alignment layers rubbed in antiparallel directions, causing the BL087, liquid-crystal material to have a slightly tilted, nematic ordering throughout the cell, with the molecules aligned almost parallel to the plates.

The first tests explored the behavior of the devices as they were exposed to high-power-laser energy. In these laser-exposure tests, the laser energy came from an IPG YLR-100-LP ytterbium-fiber laser. This fiber laser produced a TEM00 beam at 1083nm, and the output power was continuously adjustable between 0 and 100 watts. The laser was run at progressively higher output-power levels until the devices failed to function and up to its maximum value of 100 watts. The beam had a diameter of 5mm ($1/e^2$-intensity), and was carefully truncated by an aperture to ensure quality. This results in a peak intensity (in watts/cm^2) for a given laser power that is 10.19/cm^2 times the applied power in watts. Therefore, one watt of laser power results in a peak intensity of 10.19 watts/cm^2; a peak intensity of 100 watts/cm^2 corresponds to a total applied power of only 9.8 watts. In general, the peak power of a Gaussian beam is given by $2P/\pi\sigma^2$, where P is the total power in the beam and σ is the $1/e^2$ radius of the intensity pattern. Thus, when the fiber laser for this work is run at its maximum output power of 100 watts, the associated, maximum power density is around 1019 watts/cm^2. The output polarization of the laser was linear, but its orientation was not controlled for these experiments since it was only used to provide a high-power loading on the LCOPA. Exposure times were around two minutes at each power level, up to the maximum, after which the power was reduced to zero in steps. The device was mounted on a sample strip and fork mount with machined channels to permit a flow of liquid coolant. This flow, provided by a Corsair HC200-1001 coolant pump, served to stabilize the temperature of the sample. During testing, the pump was operated in its "turbo" mode. The temperature was monitored by one of two devices: an Omega HH82 digital thermometer (used with a K-type thermocouple probe) or an Extech 10-point temperature scanner, which also used a thermocouple probe. To ensure good conduction, thermal-joint compound was used at the contact points of the probes. It should be noted that these probes measured the temperature some distance away from the actual sample, and thus did not provide a completely accurate indication of the temperature at the exact point of the laser exposure.

The second tests explored the behavior of the devices when they were merely heated, with the intention of relating it to that seen in the previous tests, where any localized heating was a direct result of laser exposure. In these heating tests, the devices' temperature was repeatedly raised in 2.5°-centigrade increments until they failed to produce a measurable modulation of phase, and beyond the clearing or isotropic temperature, after which they were allowed to cool. The samples were affixed to an aluminum block heated by a thermal bar so the effects of simple heating could be investigated. The bar was controlled by an Omega CN76000 temperature controller. The temperature was monitored by the same two devices used in the first tests, in addition to the controller's thermocouple. To ensure good conduction, thermal joint compound was sandwiched between the sample strip and the aluminum heating block, as well as between the contact points of the various temperature probes. In the case of the phase shifters, at several points, as their performance began to fade or completely vanish, the drive voltage was temporarily modified in an attempt to restore functioning to the devices. It is possible that leaving the drive voltage on or off during cooling makes a difference in how and if the device resumes its normal functioning. With the intention of addressing this question, in some of the tests, the voltage was left off as the phase shifter cooled, while in others it was left on.

Before and after the tests, photographic images of the devices were recorded using a digital camera attached to a Carl Zeiss petrographic microscope. The crossed polarizers in this microscope highlighted the presence of LC material due to its birefringence. These images were intended to show any movement of the LC material in the devices caused by the conditions of the tests.

The experimental setup, as shown in figure 2, included a green, HeNe Laser (Melles-Griot 25-LGP-193-249), which was trained on the sample device. This laser had an output power of about 1mW at a wavelength of 543.5nm. The reflected beam was directed to a photodiode (Thorlabs DET210) whose output was conditioned by a Stanford-Research-Systems SR570, low-noise current preamplifier. The output was ultimately connected to a Tektronix TDS3054 oscilloscope, which is capable of saving the traces generated on its screen to files in an Excel format. While both beams struck the same point on the sample, the beam from the high-power laser followed a different path from that of the green one: the angle of incidence for the green beam was about 1.79°, while that for the high-power beam was about 10.08°. A Molectron PM300F-50 power-meter head (used with an EPM1000 control unit) served as the beam dump, as well as a monitor for the accuracy of the output-power setting of the high-power laser.

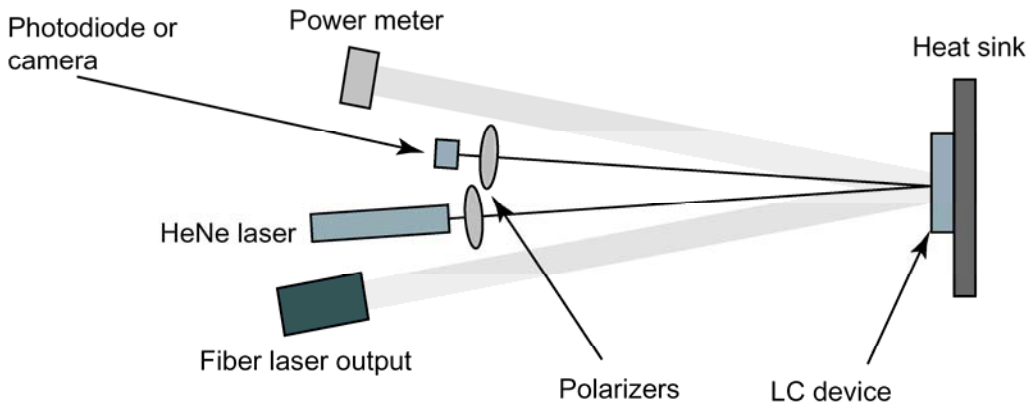

Figure 2: Schematic diagram of the LCOPA, high-power-CW-laser testing setup.

The phase shifters used in the tests were reflective, liquid-crystal cells whose back surfaces are fused silica coated with an aluminum electrode layer and covered with a reflective dielectric stack. The front surface is a piece of fused silica with an ITO coating. In these tests, the signal for the devices came from a Stanford-Research-Systems DS345 function generator, which provided a square-wave drive voltage at 1kHz, with a maximum amplitude of 10 volts, peak-to-peak, using an output-impedance setting of 50Ω. Using a ramp shape, the amplitude was swept from zero to its maximum value at a rate of 0.11 Hz.

The OPA's (SLM's) used in the tests were BNS 4096-element optical phased arrays, consisting of a VLSI-Silicon backplane, a reflective dielectric stack, an LC layer, and an ITO-coated cover glass. A detailed cross section of one such device is shown in figure 3. Each electrode is independently controllable and can be used to generate useful phase patterns for beam steering or shaping. However, in order to avoid scattering high-power-laser energy from the fiber laser, the SLM's were operated with all their electrodes at the same voltage: the device behaved as a simple phase shifter. Nevertheless, some 1μm light diffracted (presumably) from the 1.8μm-pitch-electrode pattern behind the dielectric reflective coating.

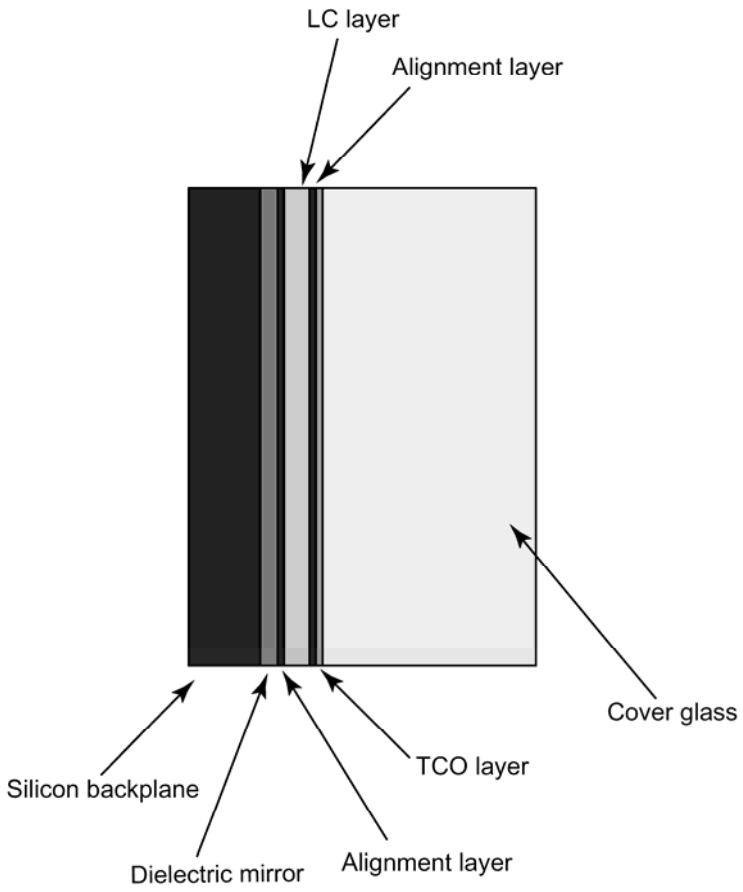

Figure 3: Schematic diagram of the layers in an LC-on-silicon device (not to scale).

In the tests using SLM's, the signal for the devices came from a computer running a LabVIEW program called "multiframe," partially written by Dr. Scott Harris, which imposes identical voltages on each pixel of the SLM, starting at zero and increasing the voltage with time to a maximum value. The only value that was entered in this program was in the next-to-bottom box labeled "milliseconds to wait", which sets the speed of the voltage sweep. This value was entered as 20ms.

In both these cases, the voltage sweep causes the devices to sweep through the values of phase shift of which they are capable. During the sweep, the LC molecules tilt so they are progressively more parallel to the light path. This presents the incoming light with a progressively-less-anisotropic, LC-molecule cross section, which results in a progressively reduced birefringent effect (reduced phase shift). The component of the light whose polarization is parallel to the slow axis of the device (along the LC molecules) is slowed down less and less, rotating the resultant polarization of the light reflected from the device. Optimally, the incoming light should have its polarization oriented halfway between being parallel and perpendicular to the slow axis of the device. A polarizer was placed immediately after the laser to adjust its polarization to this optimal angle (at about +45° relative to the slow axis of the device). A second polarizer was placed (and optimally oriented at about -45° relative to the slow axis of the device) immediately before the photodiode so the reflected light it ultimately received exhibited

intensity variations indicative of the polarization rotation resulting from the phase shift the device produced. In most cases, one oscilloscope trace was saved from a single voltage sweep for each data point. In the heating tests, these traces are intended to show the phase-shifting behavior at constant temperatures on the way up to the maximum temperature, and at constant temperatures on the way down from the maximum temperature. In the laser-exposure tests, they are intended to show the phase-shifting behavior at constant laser-exposure-power levels on the way up to the maximum exposure power of the test, and at constant laser-exposure-power levels on the way down from that maximum.

The phase shifts produced by the devices lead to the directly observed intensity variations of the oscilloscope traces. The intensity variations are essentially proportional to the cosine of the actual phase shift produced by the device. To better judge the behavior of the devices, the phase shift must be "unwrapped" from the recorded intensity variations. We created a MATLAB program to accomplish this task.

3. Results

3.1. Reduction of phase-modulation depth with laser exposure

3.1.1. Test 200312292L1 (phase shifter, laser exposure)

The oscilloscope traces in figure 4 show the behavior of phase shifter 200312292 before this test, and after exposures of 10, 20, 35, and 40 watts total laser-output power. Figure 5 shows the calculated, unwrapped phase shift before the test, and after exposures of 5, 10, 15, 20, and 25 watts. Here, the phase-modulation depth is reduced as the laser power is increased.

The traces in figure 6 show the phase modulation come back to life as the power was then lowered to 20 watts, 10 watts, and after the laser had finally been deactivated. Figure 7 shows the calculated, unwrapped phase shift for the same conditions.

Data was recorded in each case after two minutes at the indicated exposure level.

Subsequent tests, in which the maximum laser-output power was increased to 100 watts, produced essentially the same behavior in this device.

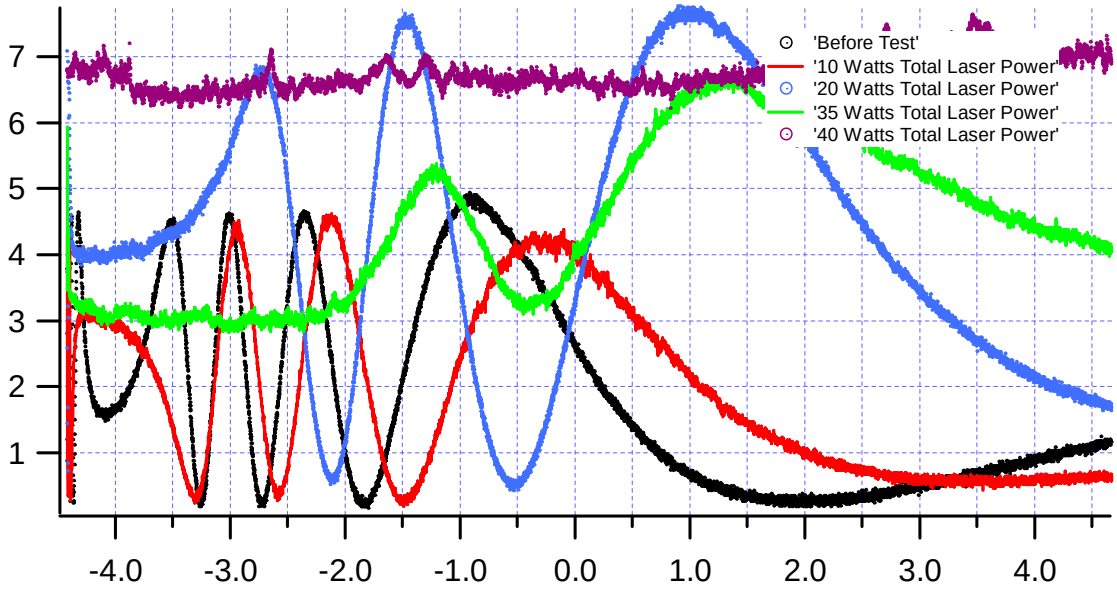

Figure 4: 200312292L1: Laser-exposure test of phase shifter 200312292 (increasing power).

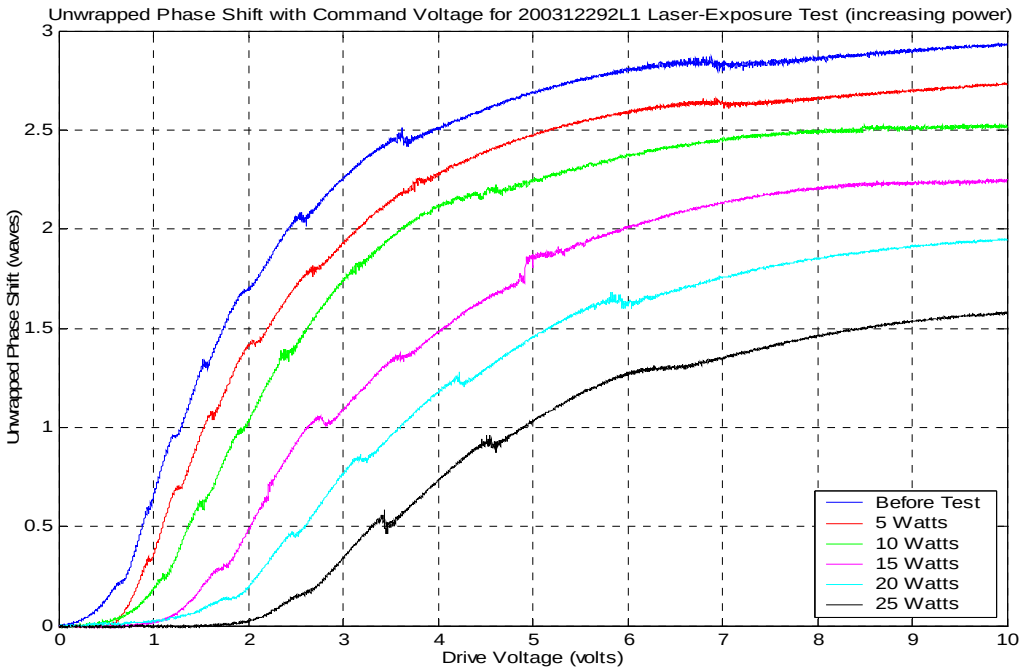

Figure 5: Unwrapped phase shift for laser-exposure test of phase shifter 200312292 (increasing power).

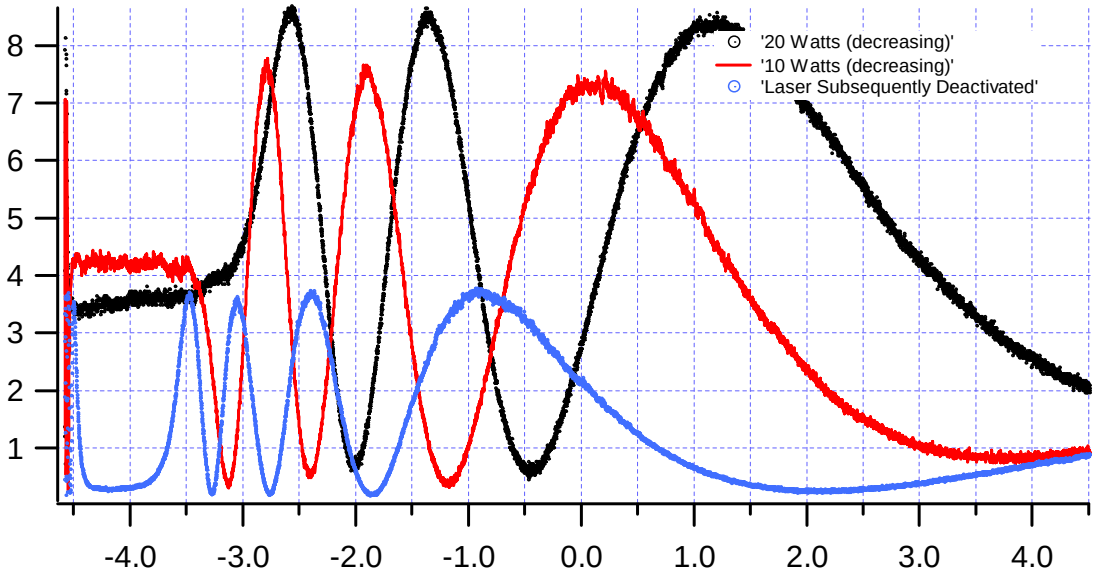

Figure 6: 200312292L1: Laser-exposure test of phase shifter 200312292 (decreasing power).

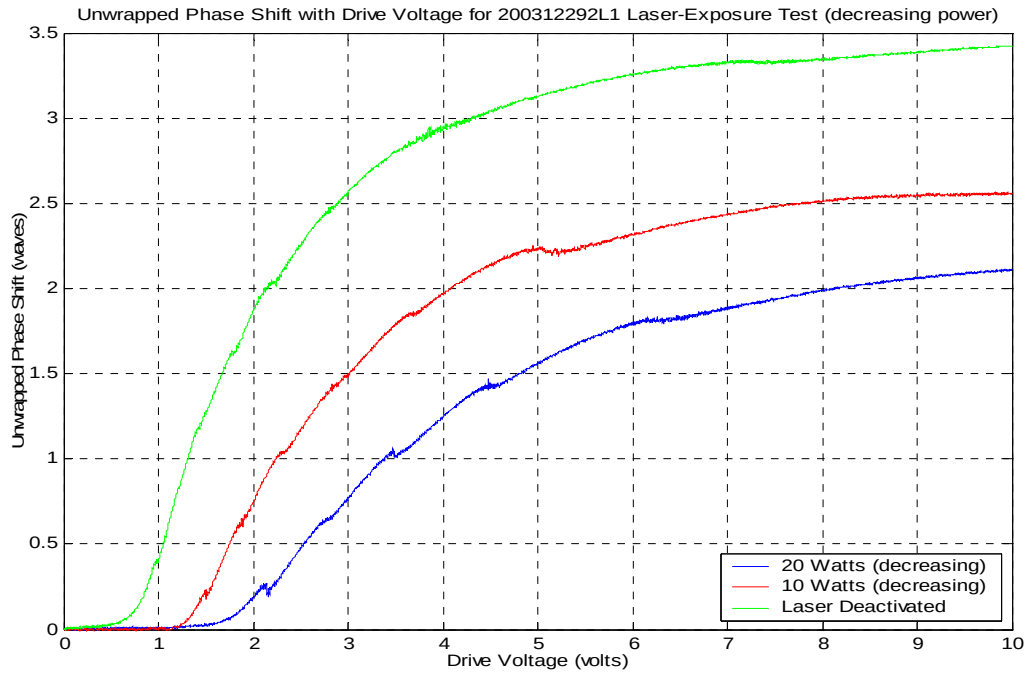

Figure 7: Unwrapped phase shift for laser-exposure test of phase shifter 200312292 (decreasing power).

3.1.2. Test 20040227L1 (spatial light modulator, laser exposure)

The oscilloscope traces in figure 8 show the behavior of SLM 20040227 before this test, and after laser exposures of 25, 50, 75, and 100 watts total laser-output power. Figure 9 shows the calculated, unwrapped phase shift for the same conditions. As in test 200312292L1, the phase-modulation depth is reduced as the laser power is increased.

The traces in figure 10, again as in the previous test, show the phase modulation come back to life as the power was then lowered to 70, 55, and 25 watts, and after the laser had been deactivated. Figure 11 shows the calculated, unwrapped phase shift for the same conditions.

As in the previous test, the data was recorded in each case after two minutes at the indicated exposure level.

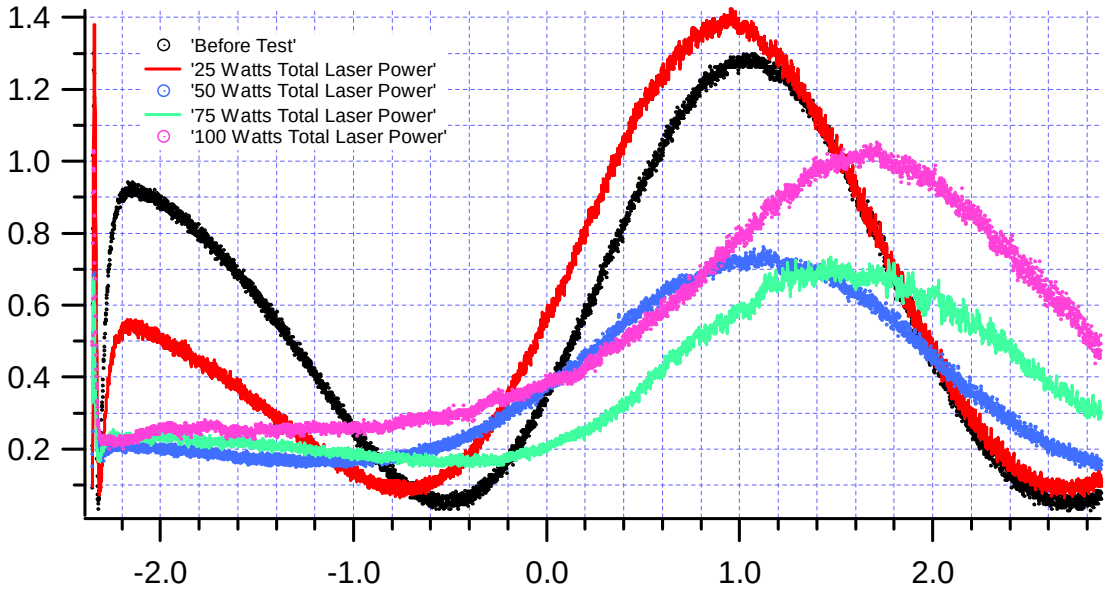

Figure 8: 20040227L1: Laser-exposure test of SLM 20040227 (increasing power).

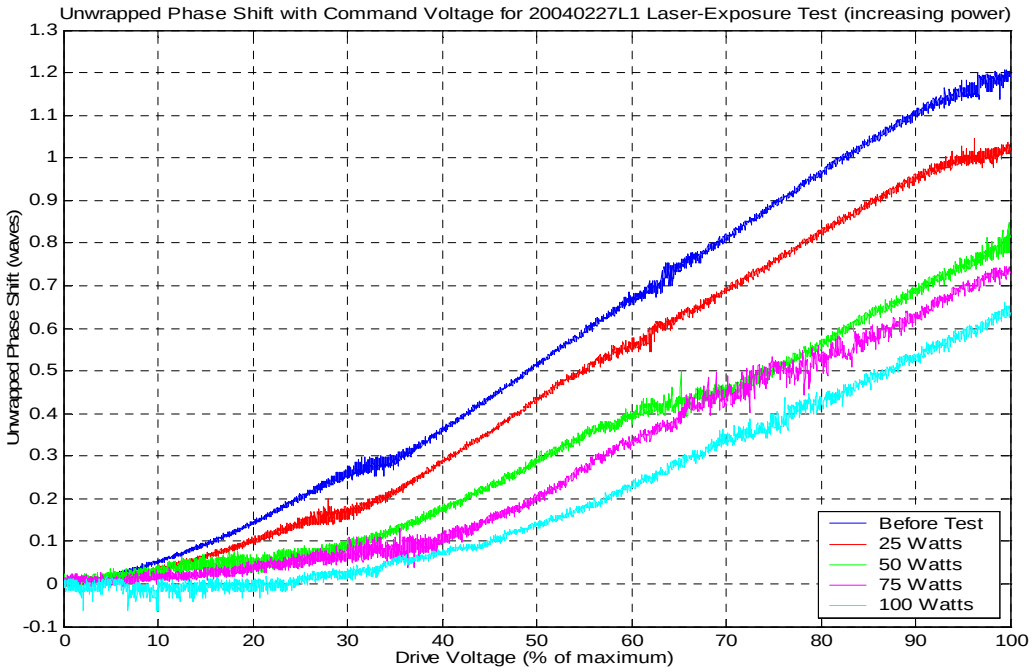

Figure 9: Unwrapped phase shift for laser-exposure test of SLM 20040227 (increasing power).

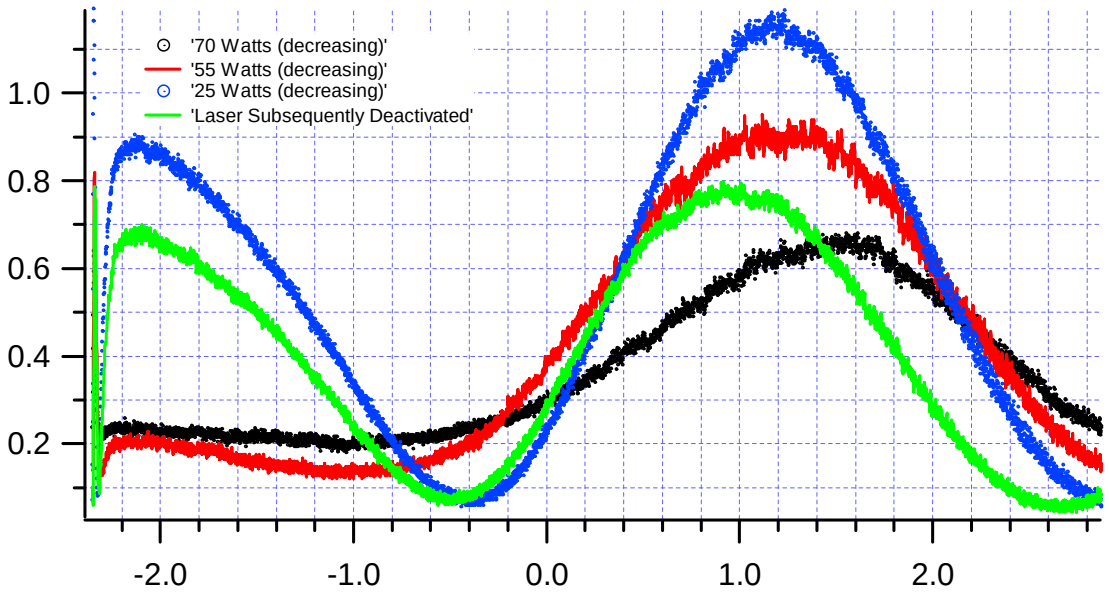

Figure 10: 20040227L1: Laser-exposure test of SLM 20040227 (decreasing power).

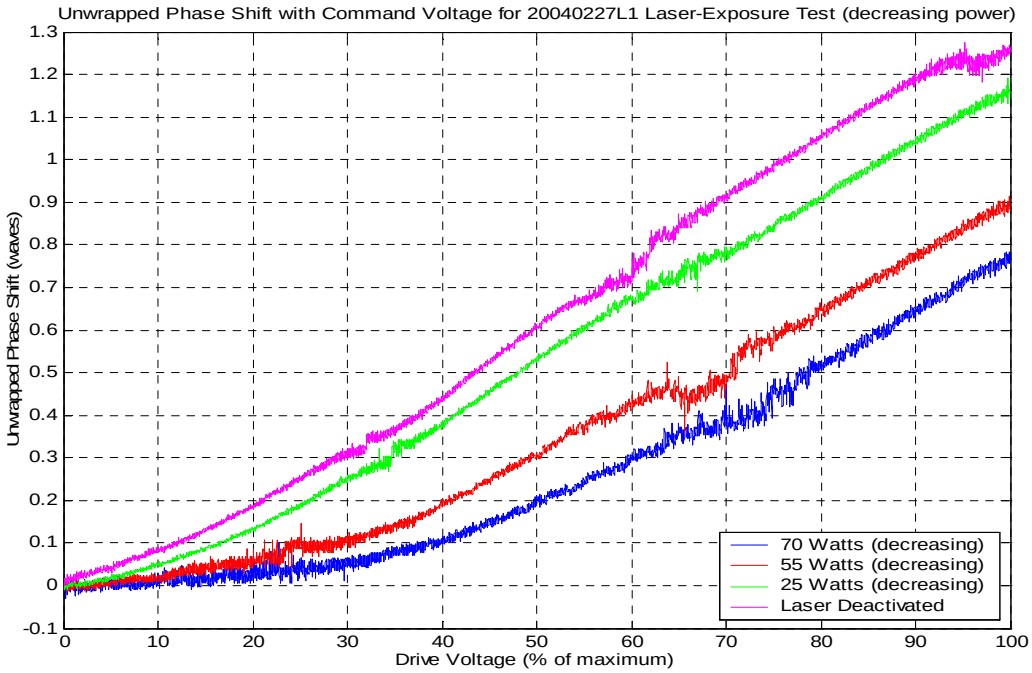

Figure 11: Unwrapped phase shift for laser-exposure test of SLM 20040227 (decreasing power).

3.1.3. Laser-exposure-test summary

These oscilloscope traces all show the transmission through crossed polarizers as the devices were swept through their full voltage ranges for various high-power-CW-laser-loading conditions. In a more succinct demonstration of the typical behavior, figure 12 shows the normalized transmission as SLM 200312191 from an earlier, preliminary test (200312191L1) was swept through its full voltage range for successively higher levels of laser power. It is clear that the phase shift produced by the device decreases monotonically as the applied power loading is increased. This can be observed by noticing that successively more peaks and troughs in the sinusoidal pattern move out of reach to the right as the applied laser power is increased. By comparing the curves that correspond to 0 watts and 10 watts (with a corresponding peak intensity of 102 W/cm^2), we can see that the phase vs. voltage characteristics of the device are essentially unchanged at this power level.

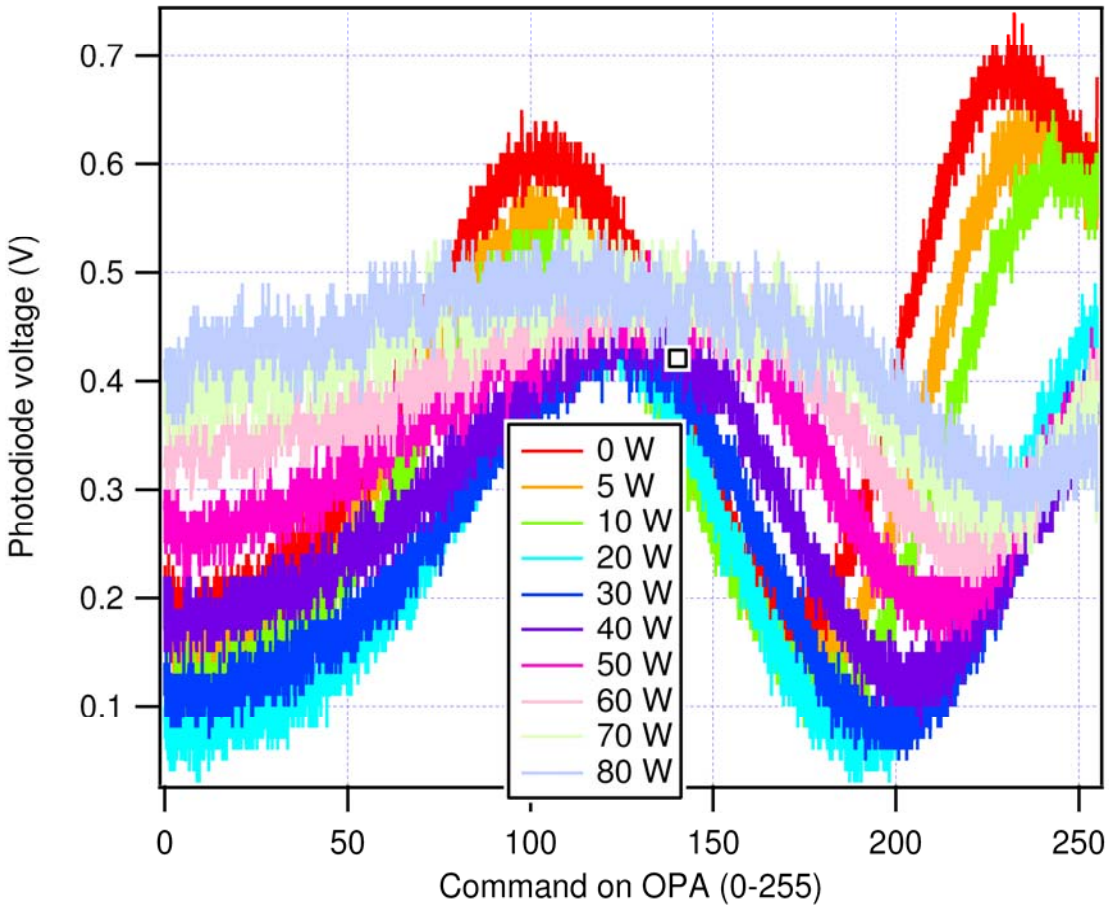

Figure 12: Normalized transmission curves for preliminary laser-exposure test of SLM 200312191 (increasing power).

3.2 Transient behavior of thermal effects

In order to investigate the temporal behavior of thermal effects in an LCOPA, the transmission curve of SLM 200312191 was recorded while the high-power laser was turned on and off. In this case, the device was operated at an intermediate voltage (i.e. the LC was NOT in a homogenous alignment).

Figure 13 shows the transient-transmission curve after the high-power illumination of 70 watts was interrupted. Clearly it takes several tens of seconds for the device to recover to its room-temperature state. The applied voltage on the LC layer in this case was half its maximum value (128/255). Figure 14 shows the transient transmission when a high-power illumination of 70 watts is instantaneously applied to the device. Again, the time required to reach steady state is several tens of seconds. In the experiment during which the laser was left on, the voltage applied to the device was 173/255 of its maximum value. The voltage applied to the LCOPA was chosen to be roughly in the middle of the available range to produce a large intensity change during the thermal transient.

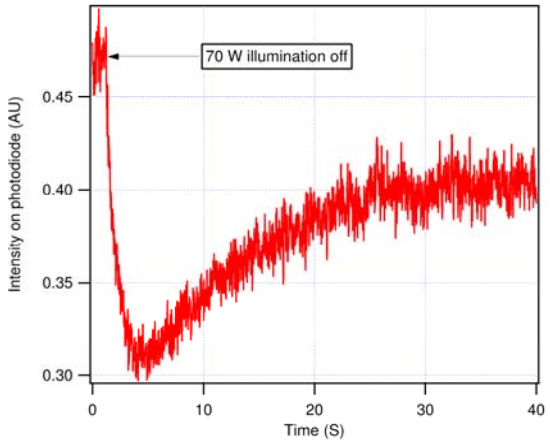

Figure 13: Cooling transient in the LCOPA when high-power illumination is turned off.

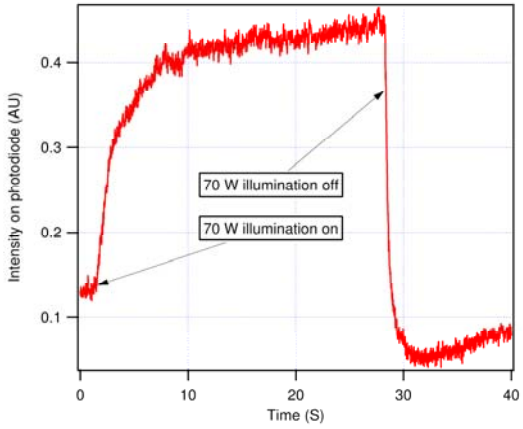

Figure 14: Heating transient in the LCOPA when high-power illumination is turned on.

3.3 Reduction of phase-modulation depth with heating

3.3.1. Test 200312193H2 (phase shifter, heating)

The oscilloscope traces in figure 15 show the behavior of phase shifter 200312193 at 19.9° centigrade before this test, and after heating it to temperatures of 39.1°, 52.1°, 67.4°, and 70.2° centigrade. Figure 16 shows the calculated, unwrapped phase shift at 19.9° centigrade before the test, and after heating the device to 39.1°, 46.9°, 49.4°, 52.1°, and 67.4° centigrade. Here, similarly to the laser-exposure tests, the phase-modulation depth is reduced as the temperature is increased.

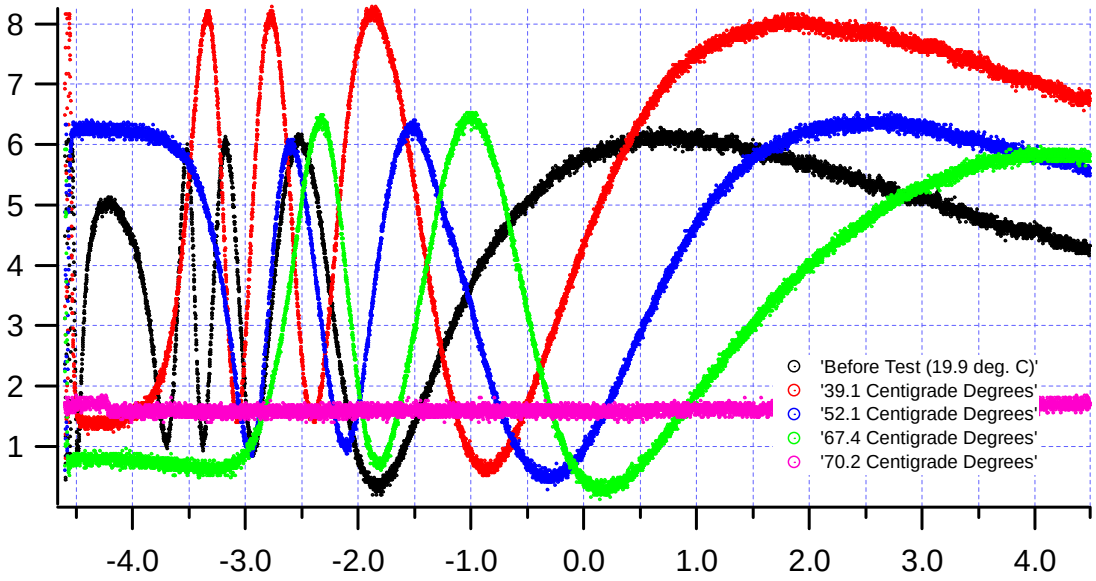

Figure 15: 200312193H2: Heating test of phase shifter 200312193 (increasing temperature).

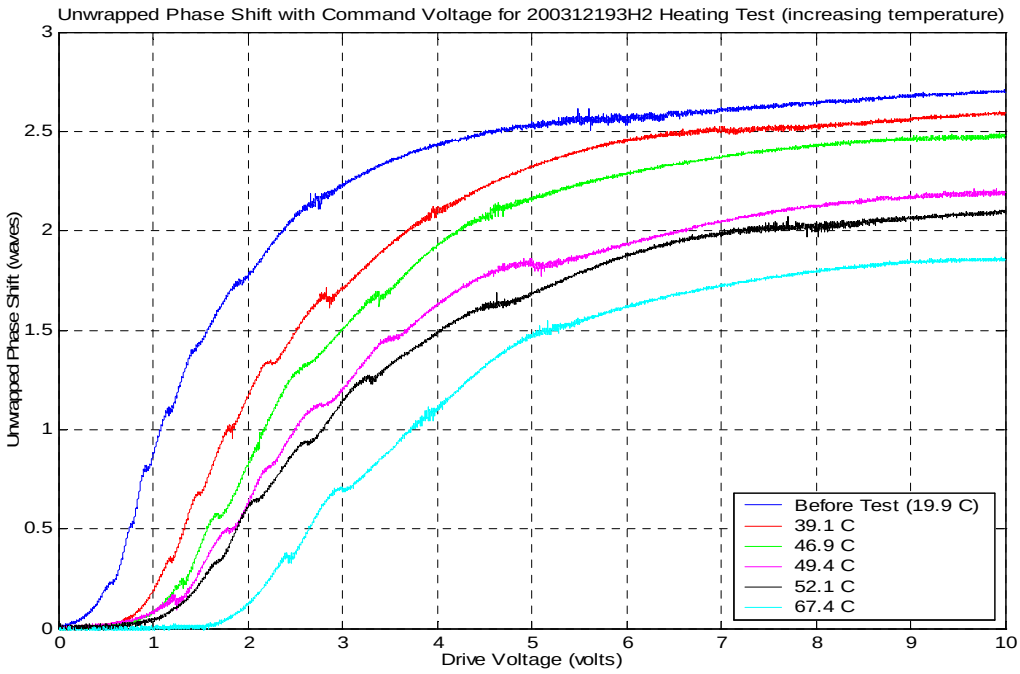

Figure 16: Unwrapped phase shift for H2 heating test of phase shifter 200312193 (increasing temperature).

The trace in figure 17 shows the behavior about ninety minutes later, when the device had cooled to 23.4° centigrade. Notice that the phase-modulation behavior essentially vanishes near 70.2° centigrade and does NOT return as the device cools.

Since this phase shifter had been heated repeatedly in an earlier, preliminary test (whose results are not documented here), these traces are from the "H2" or second heating test for this device.

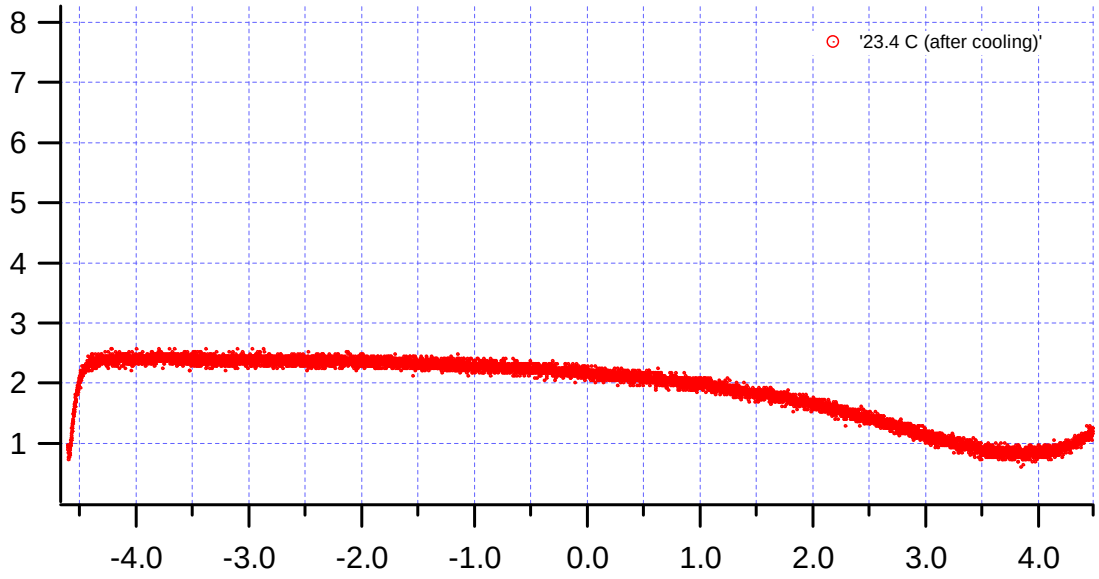

Figure 17: 200312193H2: Heating test of phase shifter 200312193 (after cooling).

3.3.2. Test 200312193H3 (phase shifter, heating; the "DC Reset")

After the end of the above test (200312193H2), a DC drive voltage was momentarily imposed on the device (a "DC Reset"), which seemed to restore its phase-modulation behavior. The device was then heated for the test runs described here in 200312193H3.

For the first part of this test, the traces in figure 18 show the behavior of the device at 22.6° centigrade before the test, and after heating it to temperatures of 51.4°, 73.6°, and 81.6° centigrade. Figure 19 shows the calculated, unwrapped phase shift at 22.6° centigrade before the test, and after heating the device to 32.5°, 43.3°, 51.4°, 66.3°, and 73.6° centigrade. As before, the phase-modulation depth is reduced as the temperature is increased. But this time, the phase-modulation behavior disappears at around 81.6° centigrade, where before it had disappeared at 70.2° centigrade. In addition to reviving the phase shifter, after its persistent demise in the previous test, the "DC Reset" seems to have extended the device's useful temperature range by more than 10° centigrade.

And, beyond that, in this test, after the initial failure, the phase modulation DID come back to life all on its own as the device subsequently cooled to 73.5°, 70.8°, and 16.4° centigrade, as shown in figure 20. Figure 21 shows the calculated, unwrapped phase shift for the same conditions.

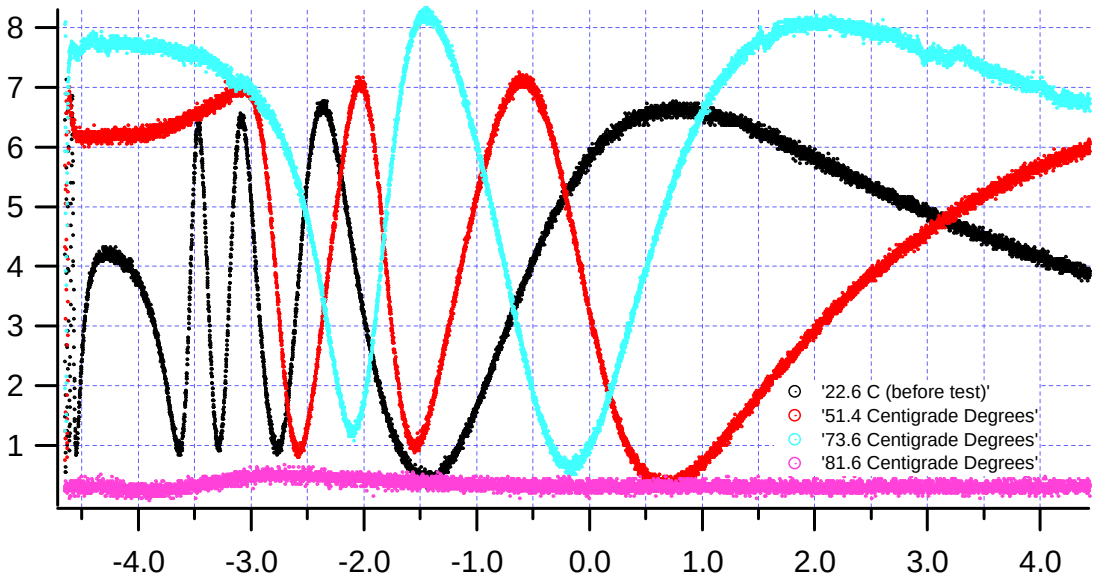

Figure 18: 200312193H3: Subsequent heating test of phase shifter 200312193 (increasing temperature). The 22.6 C trace reflects the behavior after imposing a DC drive voltage ("DC Reset") to revive the device at the end of the previous test.

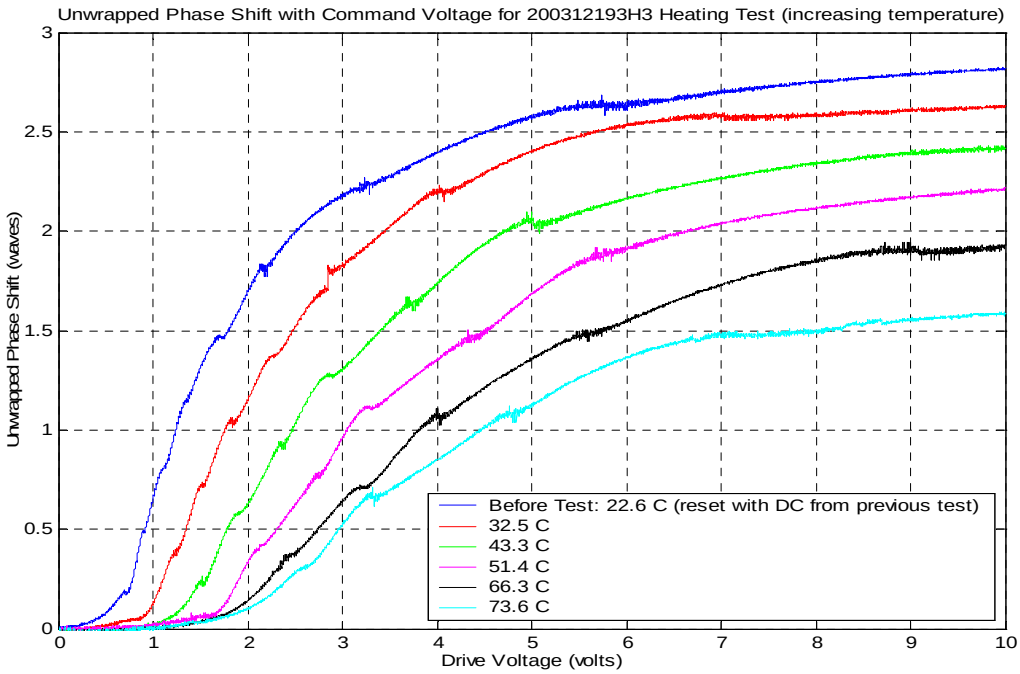

Figure 19: Unwrapped phase shift for H3 heating test of phase shifter 200312193 (increasing temperature).

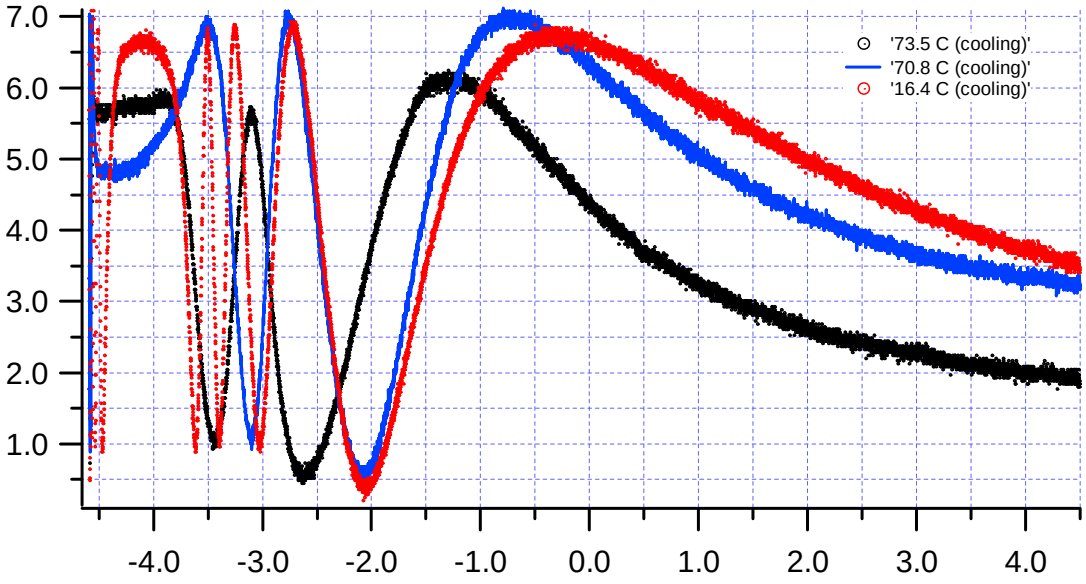

Figure 20: 200312193H3: Subsequent heating test of phase shifter 200312193 (decreasing temperature).

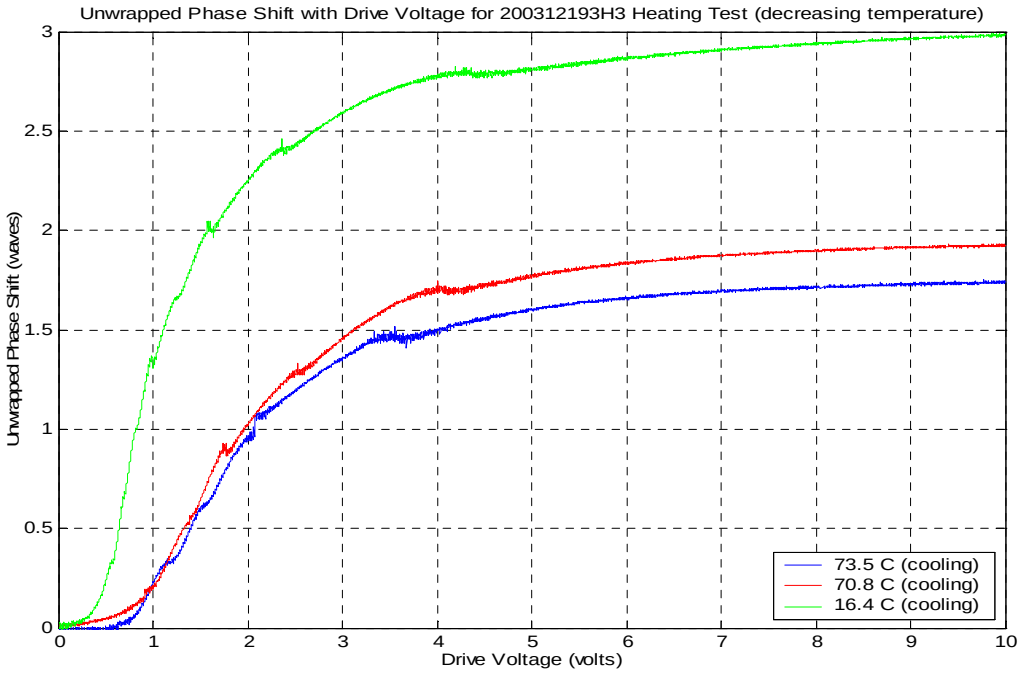

Figure 21: Unwrapped phase shift for H3 heating test of phase shifter 200312193 (decreasing temperature).

In a preliminary test performed before the 200312193H2 heating test (a preliminary test whose results are not documented here), whenever the device's phase-shifting behavior began to falter, the aforementioned DC drive voltage ("DC Reset") was momentarily

imposed, which restored or improved the device's functioning. This extended the device performance to temperature ranges beyond the point of initial failure, which occurred at a temperature of 76.2° centigrade. The usefulness of this procedure diminished at higher temperatures, and had essentially no effect at temperatures of 81.6° centigrade or higher.

In the second part of test 200312193H3, the device was heated beyond its isotropic temperature and simply allowed to cool. Normal, phase-shifting behavior returned, regardless of whether the drive voltage was left on or off as the device cooled.

The third part of test 200312193H3 was an unsuccessful attempt to reproduce the end result of the earlier, 200312193H2 test, where the device got stuck in an essentially nonfunctional state. Here the device was heated only to the point of failure and simply allowed to cool with the drive voltage left on. In this case, contrary to the outcome of test 200312193H2, the phase-shifting behavior of the device returned completely on its own as the device cooled.

3.3.3. Test 200312191L1H2 (spatial light modulator, heating)

The traces in figure 22 show the behavior of SLM 200312191 before this test, and after heating it to temperatures of 16.2° and 17.4° centigrade.

The traces in figure 23 show the behavior as heating continued to temperatures of 19.5°, 24.0°, and 26.7° centigrade.

Figure 24 shows the behavior as the temperature was further increased to 29.2°, 31.4°, 34.1°, 36.5°, 41.9°, 47.3°, and 49.6° centigrade, and after the device had subsequently cooled to 19.7° centigrade. Here, as with the heating tests on the phase shifter, the phase-modulation depth is reduced as the temperature is increased. In this case, however, the phase-modulation behavior vanishes near 49.6° centigrade, and, as in test 200312193H2, does NOT return as the device cools.

Figure 25 shows the calculated, unwrapped phase shift before the test, and after heating the device to 19.5°, 24.0°, 29.2°, and 31.4° centigrade.

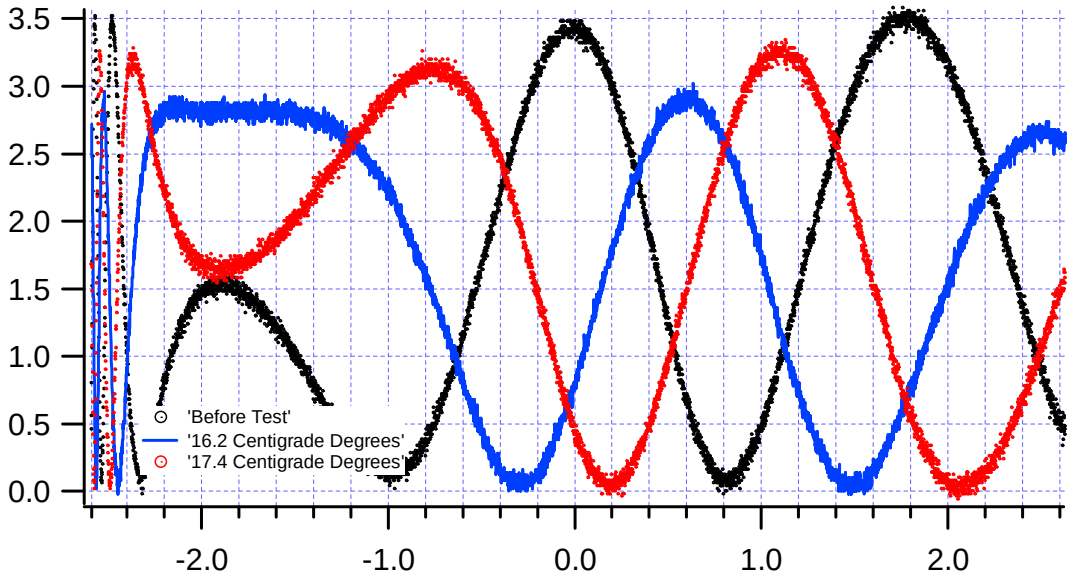

Figure 22: 200312191L1H2: Heating test of SLM 200312191 (increasing temperature).

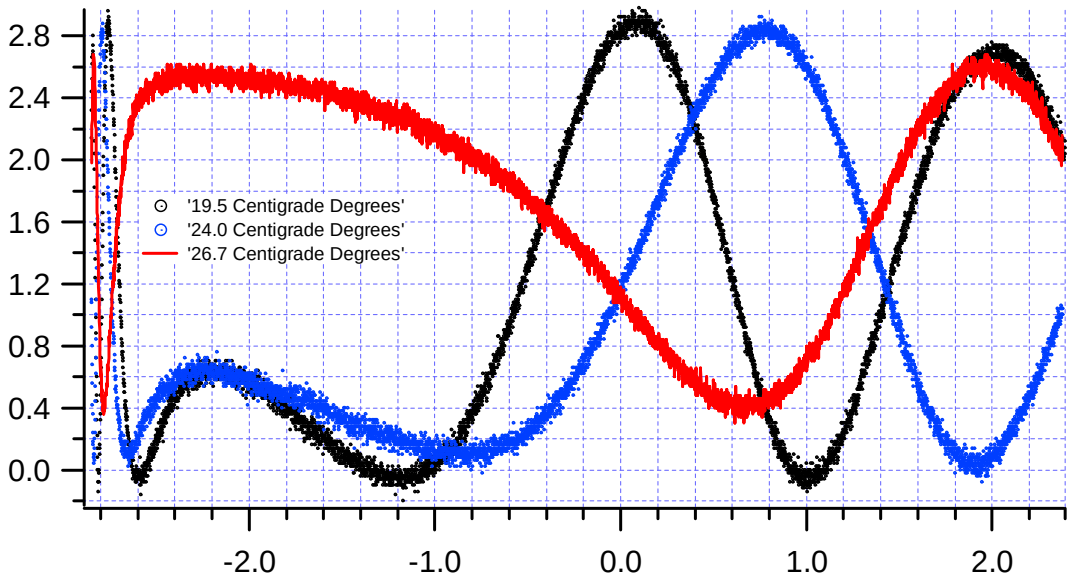

Figure 23: 200312191L1H2: Heating test of SLM 200312191 (increasing temperature).

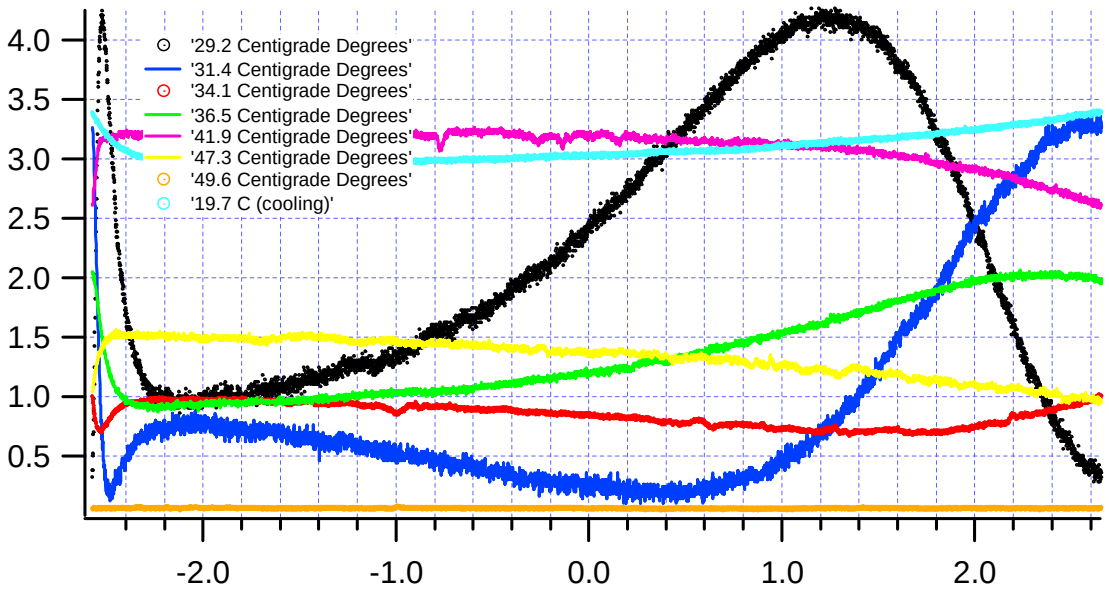

Figure 24: 200312191L1H2: Heating test of SLM 200312191 (increasing temperature, and after cooling).

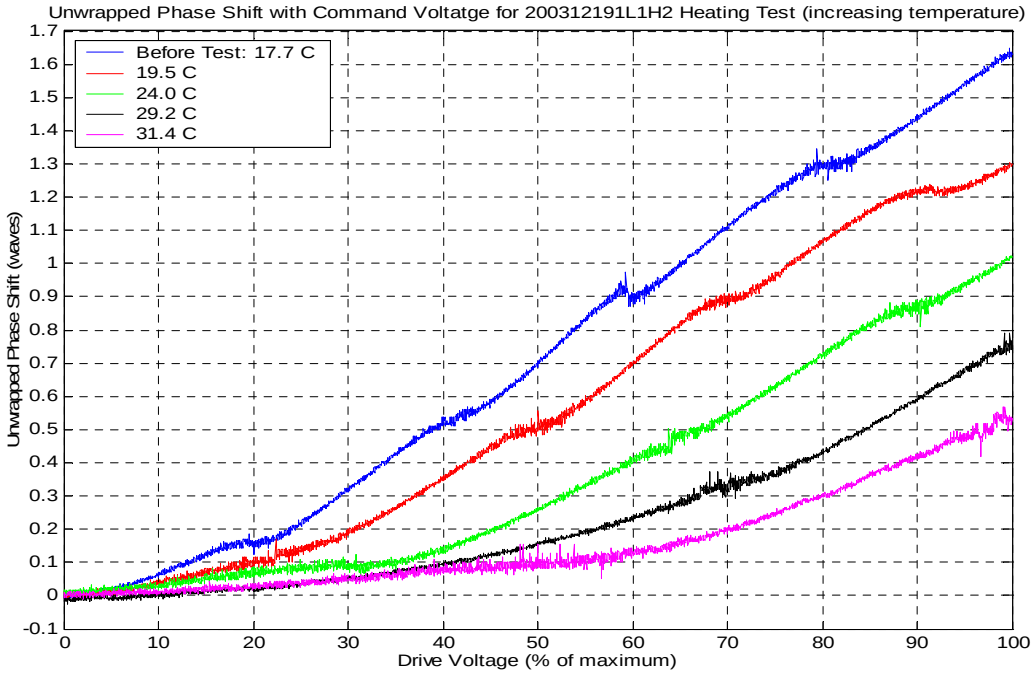

Figure 25: Unwrapped phase shift for heating test of SLM 200312191 (increasing temperature).

3.3.4. Heating-test summary

These oscilloscope traces show the transmission through crossed polarizers as the devices are swept through their full voltage ranges for various heating conditions. The intention was to compare the effects of simple heating to those produced by high-power-laser exposure at 1.083μm. In a more succinct demonstration of the typical behavior, figure 26 shows the normalized transmission curves of phase shifter 200312193 as it was swept through its full voltage range and the temperature slowly increased (from test 200312193H2). The decrease in phase throw is qualitatively the same as that observed in the spatial light modulators subjected to high-power-laser exposure.

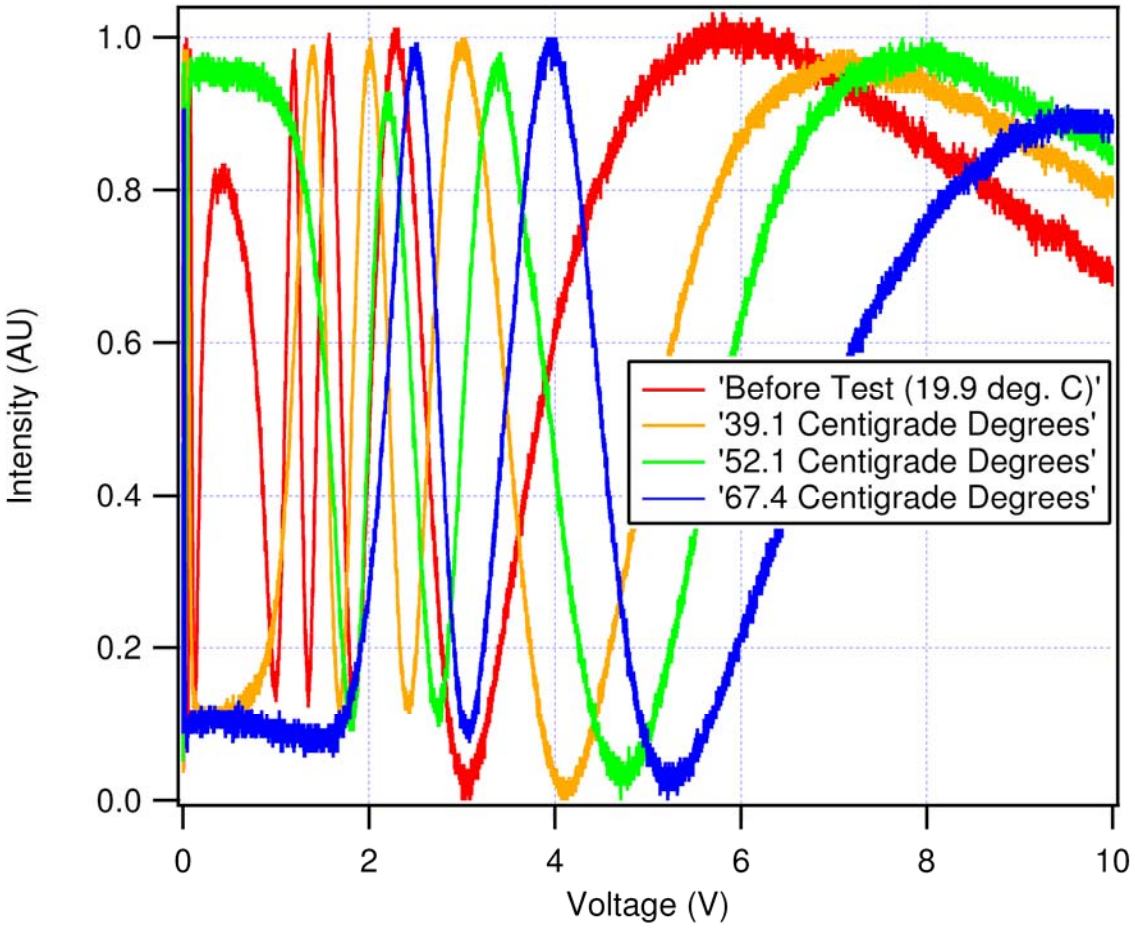

Figure 26: Normalized transmission curves for heating test of phase shifter 200312193 (increasing temperature).

When SLM's and phase shifters were heated to very high temperatures they ceased to operate. In the case of SLM's, any heating above 50° centigrade or so rendered the devices nonfunctional. The mechanism for this effect is currently not well understood. Phase shifters were also rendered nonfunctional when they were heated to very high temperatures, but the critical temperature in these cases was 70° centigrade.

In test 200312193H3, phase shifter 200312193 (rendered nonfunctional by subsequent heating in test 200312193H2) was exposed to a 0.5-Hz, 10-volt-peak-to-peak signal for around four seconds instead of the normal 1-kHz drive voltage: this procedure apparently restored the phase shifter's functionality to what it was before the heating. This sequence was repeated several times with several different phase shifters, and, in all cases, the low-frequency drive voltage restores thermally "deactivated" devices to normal operation. We speculate that the mechanism for this behavior is related to a change in the liquid-crystal alignment caused by raising the temperature above the clearing point of the liquid-crystal material. The limitations of the drive electronics for the SLM's prevented us from trying this lowered-frequency procedure with SLM's that had been similarly heated to very high temperatures.

3.4. Images through crossed polarizers

3.4.1. Apparent reduction of phase-modulation depth

In addition to quantitatively measuring the phase vs. voltage response of the device near the center of the applied high-power-CW-laser beam, qualitative images of the effects of the CW-laser beam were obtained by imaging the phase shifter or SLM under test through crossed polarizers. The same green laser was used as shown in figure 2, but in this case its beam was expanded and collimated to cover the entire device. A short-pass filter (laser-goggle lens) was placed in front of the camera to block the intense, scattered, 1.083-μm energy.

Figure 27 shows a sequence of still images of phase shifter 200312193. These images were lifted from a video segment recorded while the CW-laser power was slowly increased to its maximum value. The thermally induced change in birefringence produces a series of quasi-concentric interference fringes.

From the images in figure 27, it is clear that the high-power laser causes a localized reduction in the phase-shifting ability of the device.

Real-time-video examination of the device (being driven with a periodic signal to produce a periodic phase shift) confirmed that the central region produces a decreasing phase-modulation depth as the applied laser power is increased.

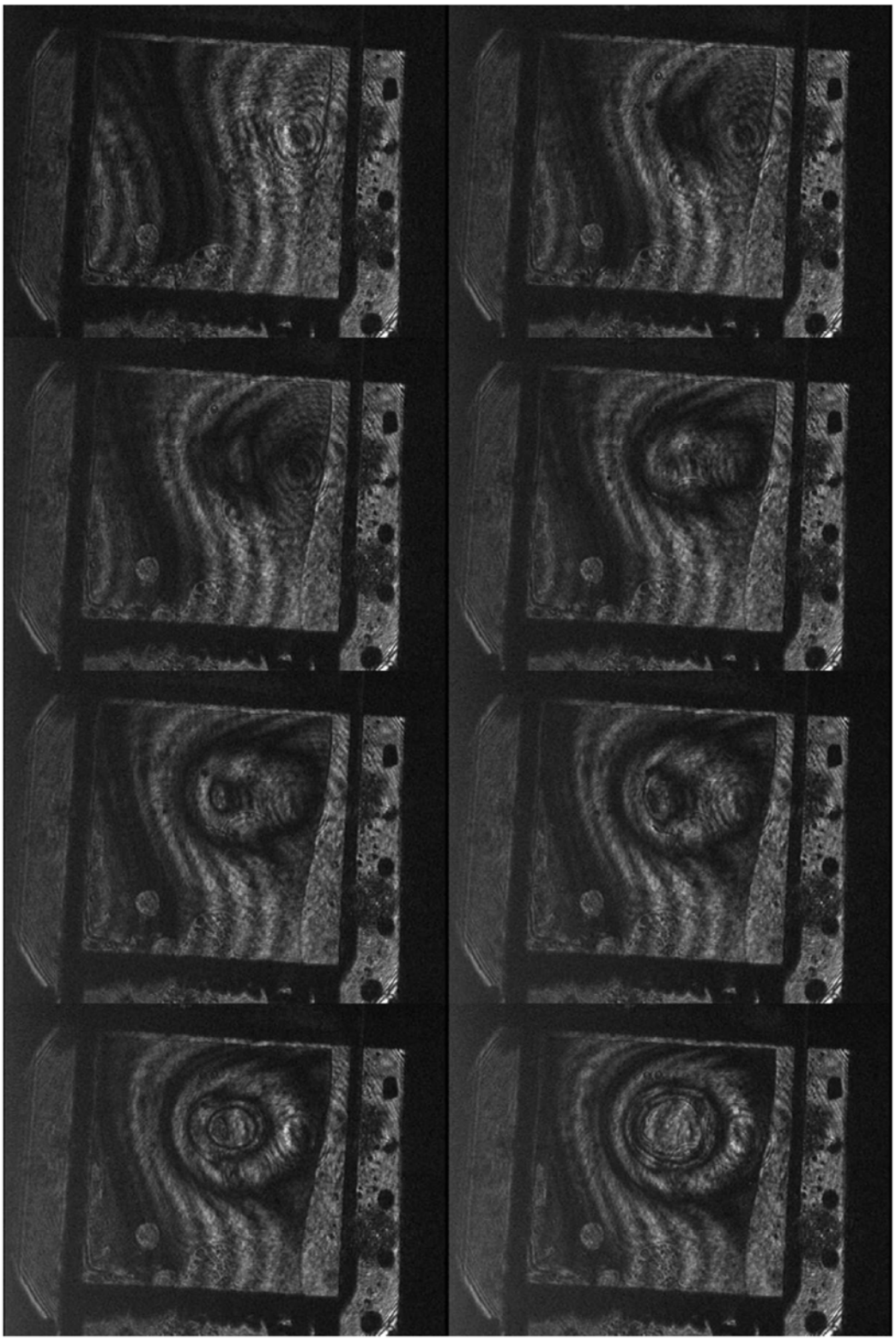

Figure 27: A sequence of images of phase shifter 200312193 recorded as the CW-laser power was slowly increased. Power levels are 0W, 30W, 40W, 50W, 60W, 80W, 90W, and 100W (left to right, top to bottom).

3.4.2. Apparent damage (reversible in some cases)

The devices examined in this effort exhibited a variety of persistent (and sometimes permanent) changes when they were exposed to extremes of temperature and laser exposure. Following the above test (which provided the images shown in figure 27), when the high-power laser was quickly turned off while the phase shifter was powered, features like that shown in figure 28 remained visible in the device. In contrast, such defects did not appear when the laser power was slowly decreased. Also, subsequent re-exposure of the spot seen in figure 28 to high laser-power levels, followed by a slow (over several minutes) decrease in the laser intensity “repaired" the device and eliminated the defect. These defects appear to be domain boundaries produced when a localized part of the liquid-crystal layer is brought above its clearing temperature and then cooled in the presence of a drive signal, with its associated electric fields.

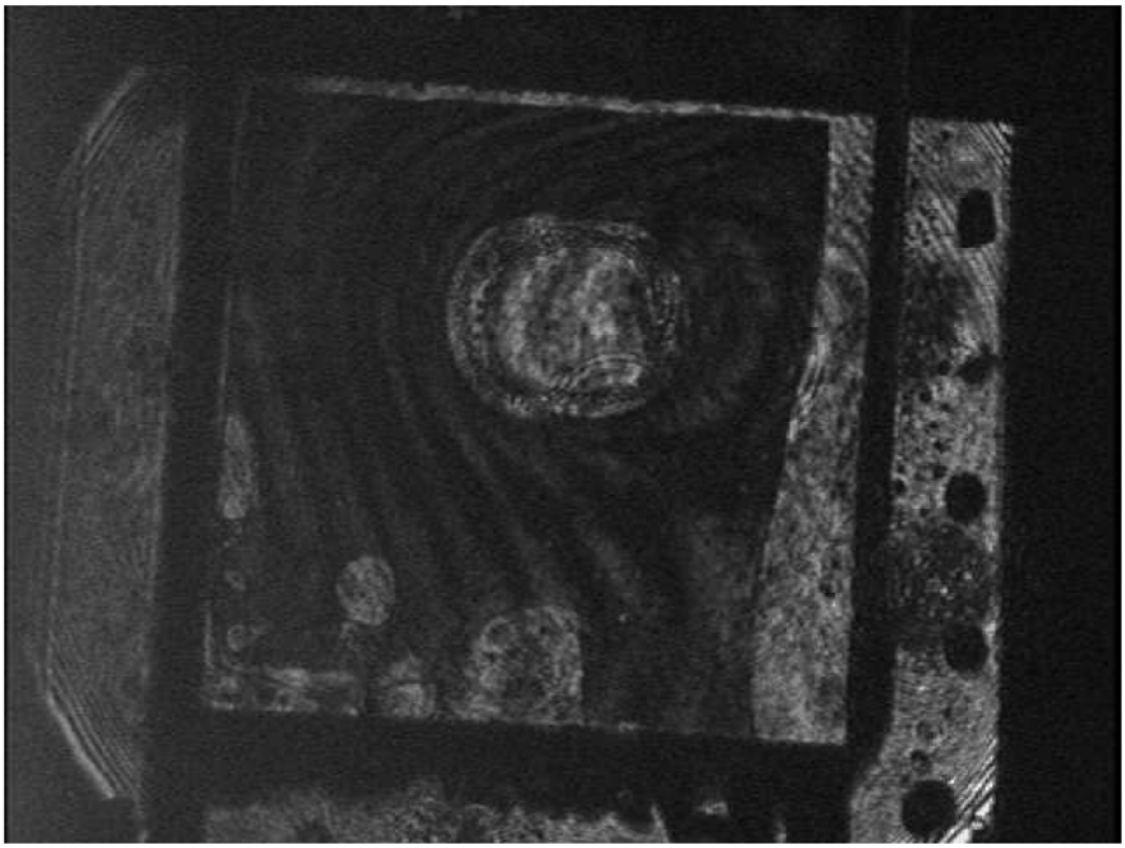

Figure 28: Persistent defect in liquid-crystal layer with continuous application of drive voltage after switching off high-power-laser illumination.

At lower laser powers (corresponding to around 102 W/cm^2), the only change observed in the devices was a minor migration of the liquid-crystal material. However, this migration was more pronounced after repeated exposure to high-power-CW-laser energy and far more prolific after thermal cycling. We assume this movement of the liquid crystal is caused by thermal expansion and contraction. Figure 29 shows petrographic-microscope pictures taken of the liquid-crystal-layer boundary of a phase shifter after a round of laser exposures and after a subsequent round of heatings. The right edge of the second picture in this figure extends to figure 30, showing the formation of a

nonfunctional void near the center of the same device. This void was likely caused by expansion and contraction of LC material due to repeated thermal cycling.

Figure 31 shows similar microscope pictures taken of the liquid-crystal-layer boundary of SLM 200312191 after a round of laser exposures and after a subsequent round of heatings.

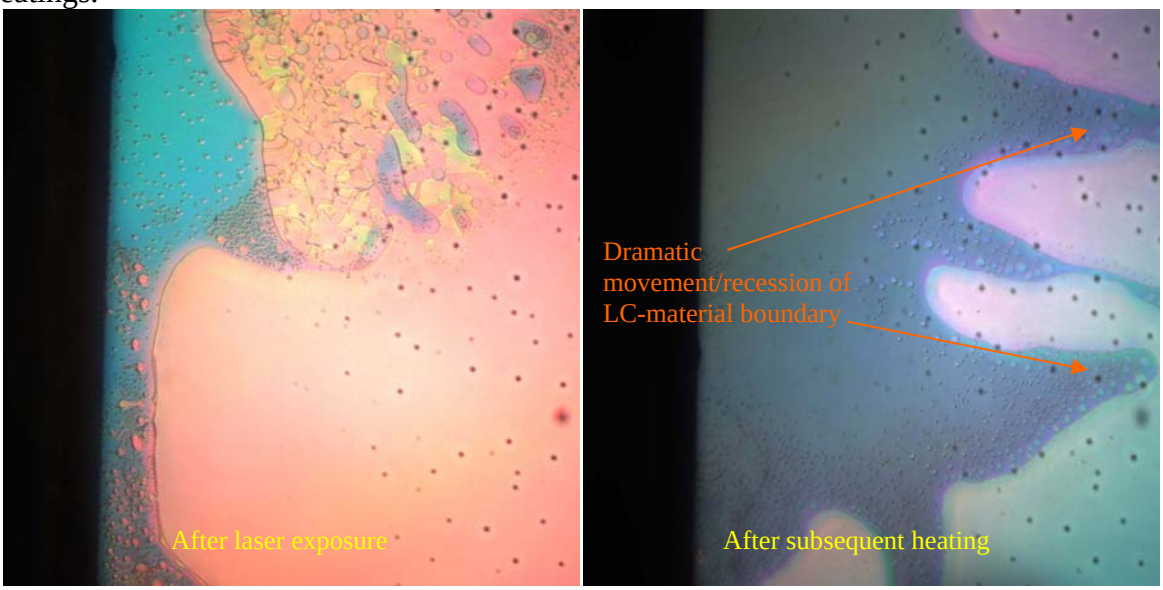

Figure 29: Petrographic-microscope pictures of liquid-crystal-layer boundary of phase shifter 200312192 after laser exposures, and after subsequent heating.

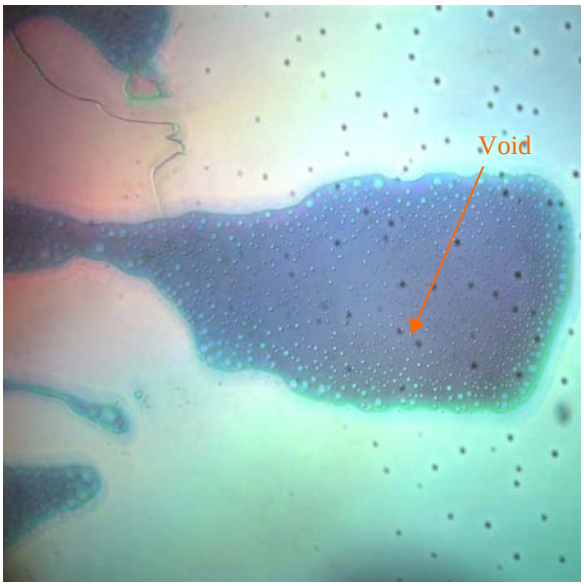

Figure 30: Extending from the right edge of the second picture in figure 29, this shows the formation of a nonfunctional void near the center of the device, resulting from movement/recession of LC material, presumably due to repeated thermal cycling.

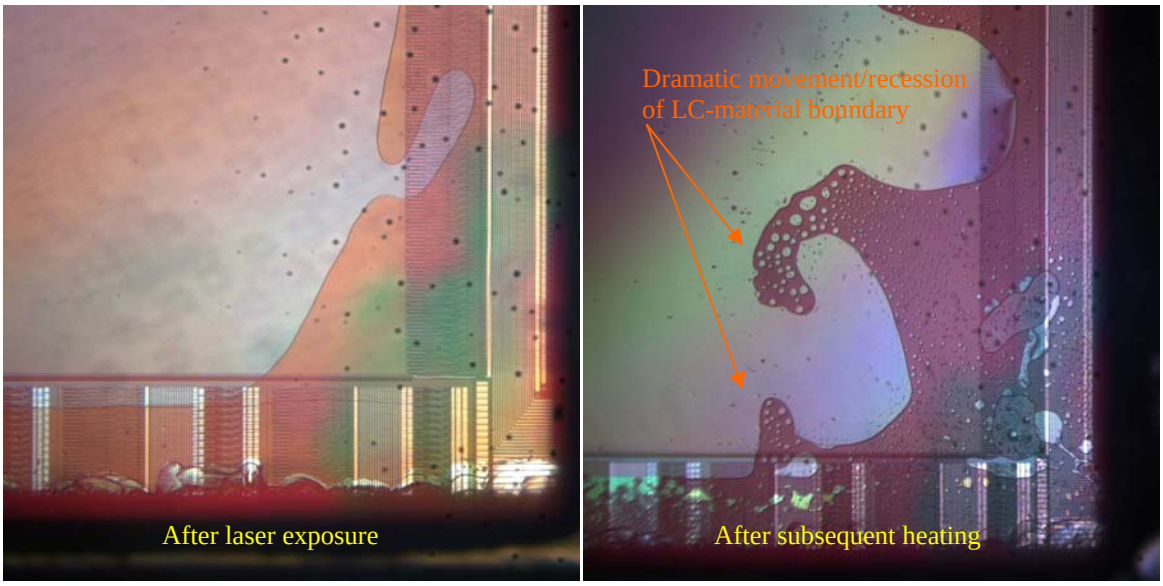

Figure 31: Petrographic-microscope pictures of liquid-crystal-layer boundary of SLM 200312191 after laser exposures, and after subsequent heating.

We did not observe any obvious visual damage to the cover glass or backplanes in any of the devices used in this work.

4. Thermal Modeling

In order to better understand the thermal behavior of LCOPA's, we consider a one-dimensional model of heat diffusion in a liquid-crystal device. The temperature distribution in an inhomogeneous, layered material is given by the familiar heat equation shown in equation 1.

$$\sigma\rho\,{}^{du}/_{dt} = {}^{d}/_{dx}\,(K\,{}^{du}/_{dx}) \tag{1}$$

K is the thermal conductivity of the material, ρ is the density, σ is the heat capacity, and u(x,t) is the temperature. If we restrict our attention to the steady-state temperature distribution in a layered structure composed of homogenous layers, in regions where no heat is being absorbed, we find that

$$K\,d^2u/dx^2 = 0. \tag{2}$$

Equation 2 only admits solutions of the form

$$u(x) = c_1\,x + c_{2.} \tag{3}$$

At each boundary between layers there are two conditions that must be satisfied. The first condition is that the temperature distribution be continuous. The second condition is that the heat fluxes across the boundary match. In this model, we assume that all of the thermal absorption takes place in infinitely thin layers between the material boundaries:

$$K_1\,({}^{du}/_{dx})_{right} - K_2\,({}^{du}/_{dx})_{left} + q_{source} = 0. \tag{4}$$

If we assume that all the heat deposited in the LC cell is removed through the backplane and that radiation and convection from the front of the device are both negligible, we can arrive at a simple procedure for evaluating the temperature distribution inside the device. Since no heat can travel to the right and exit through the cover glass, the temperature gradient to the right of the heat absorption must be zero. This implies that the temperature in the cover glass is constant. To the left of the heat source, the slope of the temperature profile is linear and is simply given by

$$K\,{}^{\Delta u}/_{\Delta L} = Q/A. \tag{5}$$

In other words, the temperature drop across each layer must be such that the deposited heat flows toward the heat sink. The temperature rise in each layer is proportional to ${}^{\Delta L}/_{K}$. A simplified temperature profile typical of this behavior is shown in figure 32.

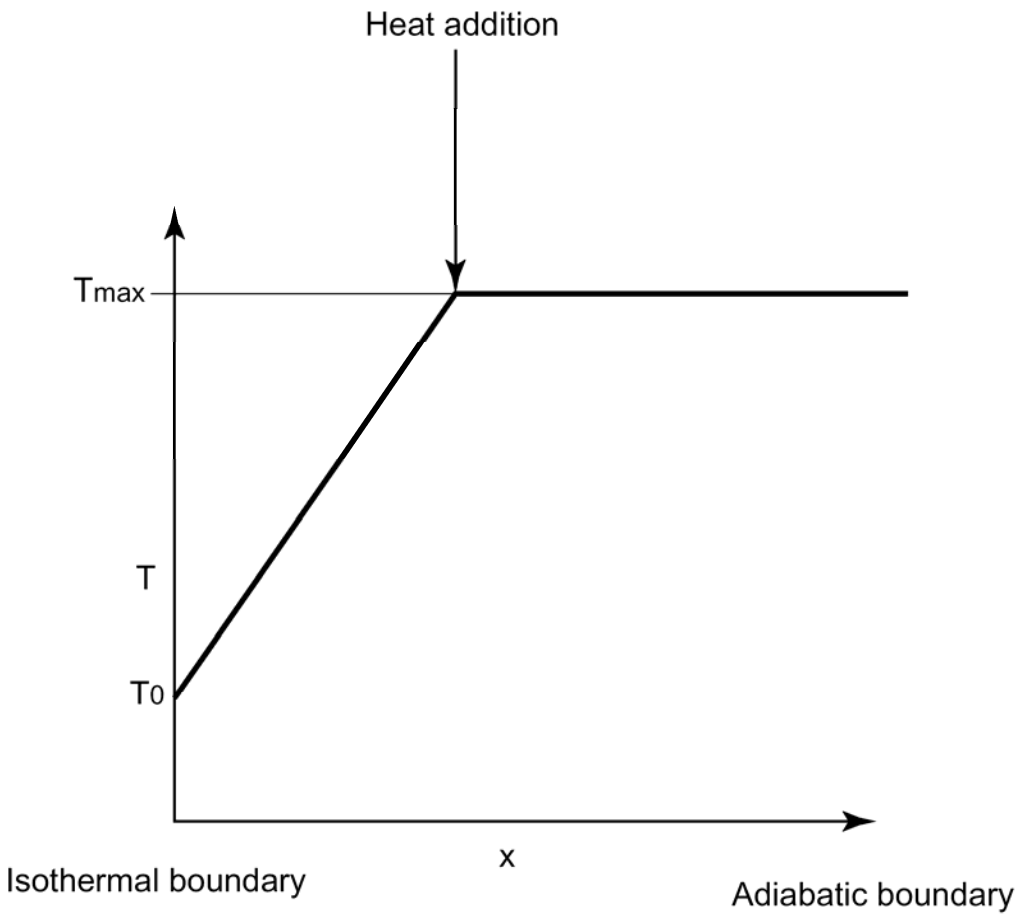

Figure 32: Simplified heat profile in an LCOPA device with one adiabatic boundary, one isothermal boundary, and heat addition taking place in a thin layer.

For a given layer, the temperature drop will be

$$\Delta u = {}^{\Delta LQ}/_{KA}, \tag{6}$$

where Q/A is the power deposited in units of W/cm^2 and ΔL is the thickness of the layer. Looking at table 1, it is clear that the temperature rise in the LC layer will dominate the overall temperature rise of the device. The thermal conductivity of the LC layer is estimated to be the same as for an organic solvent.

Material	Thermal conductivity	Thickness	$\Delta L/K$
LC	$0.2\ W/(mK)$	$7\ \mu m$	3.5×10^{-5}
Silicon	$138\ W/(mK)$	$720\ \mu m$	5.2×10^{-6}
Fused Silica	$13\ W/(mK)$	$2000\ \mu m$	1.5×10^{-4}

Table 1: Thermal conductivity for materials in a typical LCOPA.

The actual thermal loadings required to produce a 100-K temperature rise across a layer in an LCOPA are shown in table 2. The cover-glass layer in the device is its most insulating layer, but since it is an adiabatic boundary, it plays no role in determining the internal temperature of the device.

Material	Required thermal load for 100 K temperature rise
LC	286 W/cm^2
Silicon	1900 W/cm^2
Fused Silica	65 W/cm^2

Table 2: Required heat absorption for a 100-degree-C temperature rise across a material layer in an LCOPA.

5. Conclusions

5.1. Reduction of Phase-Modulation Depth

For these devices, as the temperature or laser power was raised, three main effects were observed: the unwrapped-phase-shift plots clearly show that the available phase-shift depth decreased; the onset of the greatest slope of phase shift with voltage change occurred at higher voltage values; and the magnitude of the greatest slope of phase shift with voltage change decreased.

While the unwrapped-phase-shift plots for the phase shifters showed a leveling off at higher voltages, those for the SLM's did not. The likely reason for this was the limited voltage range of the drive electronics used with the SLM's: this meant that those devices were operated in a drive-voltage range that was narrower than optimal.

This phenomenon may warrant further explanation. At first, as the voltage is increased, the LC molecules stay put in their neighbor-interaction-induced positions. Once the voltage (field) reaches a particular threshold value (at what is often referred to as the Friedricsz Transition), the molecules break free from these positions and begin to tilt; from here, the phase shift increases rapidly as the voltage is increased. The long moment arm presented by the LC molecules adds to this rapidity. In the case of an appropriately chosen drive-voltage range, as the device reaches its maximum phase-shift value, the LC molecules reach their maximum tilts, presenting progressively shorter moment arms for the field-induced torque as they rotate. This means that, while the initial phase-shift increase is rapid, as the maximum phase-shift value is approached, the phase-shift increase slows down. This is why the unwrapped-phase-shift curves level off at higher voltages in the phase-shifter tests.

In contrast, if the drive-voltage range is chosen with its maximum value lower than optimal, the molecules never reach a tilt where the phase-shift increases become less rapid. This is the likely reason the unwrapped-phase-shift plots for the SLM's do not level off at higher voltage values.

5.2. Migration of liquid-crystal material

As the samples are heated, or exposed to high-power-laser energies, it is clear that the LC material moves around. In one case, for which images were not recorded, the movement of the LC material was observed in situ during the heating and cooling. In this instance, it was clearly visible that, as the temperature was raised, the LC material irregularly receded inward from the device edges, and as it cooled, irregularly crept back out toward the edges. In some cases, this repeated, irregular recession and creeping back can cause a sort of dent in the LC boundary along the edge of the device. Successive thermal cycles, with the associated, irregular, LC-material movement, can cause such a dent to deepen, and the more expanded borders around it to close in upon it, ultimately forming a void of air near the center of the device, like that shown in figure 30. In this case, the void was so large that the behavior of the device only within the void could be observed, which showed a completely impaired phase-shifting behavior. Using sections of the device on either side of this void provided normal phase-shifting behavior.

Keeping in mind the construction of these devices (as explained above in section 1.2. Beam-steering overview), it is thought that the eventually destructive LC-material movement is due to thermal expansion and contraction of the spacers and glue.

More specifically, as the temperature is raised, it is unlikely that the LC material expands as much as the glue and spacers. As they expand, these components push the glass plate away from the backplane: the volume of LC material is no longer sufficient to fill the entire volume between these two surfaces. Air enters through any unsealed gaps in the glue line around the device perimeter to fill the additional volume. Subsequent cooling contracts the spacers and glue, pulling the glass plate back toward the backplane. This pushes out some of the air, as well as some LC material which had perhaps crept around in front of it. The result is that every thermal cycle likely results in less LC material (as well as more air voids) inside the functional area of the device. What one would expect to observe in this scenario is exactly what appears to happen when the device is heated and cooled. Ultimately, repeated thermal cycles will likely cause the eventual failure of any of these devices constructed in this way.

It should be noted that the LC-material movement in the heating tests is more prolific than in the laser-exposure tests. This is likely due to the fact that the thermal effects in the latter are more restricted ONLY to the small area of the laser exposure, whereas in the former, the ENTIRE device, including the LC material, spacers, glue, and glass plates warms up, setting the stage for a greater aggregate effect.

When phase shifter 200312192 was heated, LC-material movement formed a void which impaired its function, at least in that specific region. However, in the SLM-heating test 200312191L1H2 (and to a less prolific degree, phase-shifter-heating test 200312193H2), device failure was brought on by a mechanism other than void formation. It is possible that failure in those cases came about from an overall, thermal disorientation of the LC molecules. As a testament to this possibility, in the phase-shifter case, the imposition of a momentary DC drive voltage (“DC Reset”) brought this device back to life for its next heating test, 200312193H3. Unfortunately, because of hardware limitations, it was not possible to impose a DC drive voltage on SLM 200312191 after it was similarly incapacitated by heating. Thus, this “DC-Reset” method of restoration could not be attempted with that device, and SLM 200312191 remains essentially nonfunctional to this day.

5.3. Summary of Conclusions

We have demonstrated that reflective liquid-crystal optical phased arrays can easily operate at CW-laser-exposure intensity levels of up to 102 W/cm^2 without any difficulty. At higher power levels, the heating caused by absorption of the laser energy causes two adverse effects. First, the locally elevated temperatures cause a reduction of the liquid-crystal birefringence and eventually drive the liquid-crystal layer to its isotropic state. Second, the repeated, extreme heating and cooling cycles caused by the high-power-laser exposure appear to cause the liquid-crystal material to migrate inside the device. We speculate that this phenomenon can be controlled with either better seals around the cell edges or a feature specifically designed to permit the liquid-crystal material to freely expand and contract within a reservoir. Exposure to high temperatures appears to damage the devices in a way that, while similar to that caused by high-power-laser exposure, is currently not well understood.

We developed and explored a novel technique of restoring functionality to a phase shifter once it has been persistently impaired by heating. This “DC Reset” technique also permits the performance of phase shifters to be extended to temperature ranges beyond the point of initial failure.

Finally, we presented a simple one-dimensional thermal model for a liquid-crystal optical phased array that allows us to estimate the importance of different materials in specific regions of such a device relative to the temperature distribution within it.